

ALMA MATER STUDIORUM - UNIVERSITÀ DI BOLOGNA  
CAMPUS DI CESENA  
SCUOLA DI INGEGNERIA E ARCHITETTURA

CORSO DI LAUREA MAGISTRALE IN INGEGNERIA BIOMEDICA

BIOMECHANICS OF THE DISTAL  
RADIO-ULNAR JOINT: FINITE ELEMENT  
STUDY

TESI IN

MECCANICA DEI TESSUTI BIOLOGICI

Relatore

*Prof. Luca Cristofolini*

Presentata da

*Alessandra Procopio*

Correlatore

*Prof. Paolo Gargiulo*

*Prof. Magnùs Kjartan Gislason*

III° Sessione

Anno Accademico 2012/2013

*Ai miei Genitori...*

<b>ABSTRACT</b> .....	<b>3</b>
<b>1. Introduction</b> .....	<b>5</b>
<b>1.1 Anatomy and Function</b> .....	<b>5</b>
<b>1.2 Segmentation methods, Morphologic and Boolean         Operations</b> .....	<b>8</b>
<b>1.3 Finite Element Model</b> .....	<b>10</b>
<b>1.4 Aim</b> .....	<b>16</b>
<b>2. Material and Methods</b> .....	<b>17</b>
<b>2.1 Defining the geometry</b> .....	<b>17</b>
<b>2.1.1 Radius and Ulna Bones</b> .....	<b>17</b>
<b>2.1.2 Cartilage</b> .....	<b>21</b>
<b>2.2 Meshing the cartilage and bones</b> .....	<b>23</b>
<b>2.3 Ligaments</b> .....	<b>25</b>
<b>2.4 Tissue properties Modeling</b> .....	<b>28</b>
<b>2.5 Finite Element Analysis</b> .....	<b>29</b>
<b>2.5.1 Model Constrains</b> .....	<b>31</b>
<b>2.5.2 Specification of loading conditions</b> .....	<b>32</b>
<b>2.6 Fracture Risk Analysis</b> .....	<b>35</b>
<b>3. Results</b> .....	<b>36</b>
<b>3.1 Verification of 3D Models</b> .....	<b>36</b>
<b>3.2 Verification of stress and strain simulations</b> .....	<b>39</b>
<b>3.3 Clinical Aspects</b> .....	<b>42</b>
<b>4. Discussion</b> .....	<b>44</b>
<b>5. Conclusion</b> .....	<b>48</b>

<b>References .....</b>	<b>49</b>
<b>Acknowledgments.....</b>	<b>54</b>

# ABSTRACT

The finite element method has been employed with considerable success to explore load distribution and deformation patterns at a variety of locations in the human body. The finite element method has had less impact on knowledge of the mechanics of multi-bone joints such as the wrist.

The aim of the project was to evaluate the clinical e biomechanical aspects of the distal radio-ulnar joint, through the use of modeling methods and finite element analysis.

Two 3D models are designed from DICOM CT-images. Images belonged to a patient with healthy joint and a patient with pathologic joint; in particular, the pathology is caused by a traumatic dislocation of the ulna.

The main components of models were: radius, ulna, cartilage, interosseous, palmar and distal ligaments.

Segmentation methods of “Thresholding” and “RegionGrowing” are used to realize the radius and ulna; thanks to Morphologic and Boolean Operations, it is possible to distinguish the cortical and the cancellous bones. Subsequently, the cartilage between two bones is created through Boolean Operations. Instead, ligaments are designed by taking the node-points of the radius and ulna, then the area through them is formed.

For each component, the corresponding material properties are assigned. To improve the quality of models, it was necessary to apply operations of “Smoothing” and “Remesh”.

Following, a Finite Element Analysis is performed through the use of supports and forces, which can simulate the behavior of two joints. In particular, the stress and strain are simulated.

Finally, through the results obtained from simulations, it was possible to assess the possible risk of fracture in different anatomical points of healthy and pathological joints.

# ABSTRACT

Il metodo agli elementi finiti è stato utilizzato per valutare la distribuzione dei carichi e delle deformazioni in numerose componenti del corpo umano.

L'applicazione di questo metodo ha avuto particolare successo nelle articolazioni con geometria semplice e condizioni di carico ben definite, mentre ha avuto un impatto minore sulla conoscenza della biomeccanica delle articolazioni multi-osso come il polso.

Lo scopo di questo lavoro è quello di valutare gli aspetti clinici e biomeccanici dell'articolazione distale radio-ulnare, attraverso l'utilizzo di metodi di modellazione e di analisi agli elementi finiti.

Sono stati progettati due modelli 3D a partire da immagini CT, in formato DICOM.

Le immagini appartenevano ad un paziente con articolazione sana e ad un paziente con articolazione patologica, in particolare si trattava di una dislocazione ulnare traumatica.

Le componenti principali dei modelli presi in considerazione sono stati: radio, ulna, cartilagine, legamento interosso, palmare e distale.

Per la realizzazione del radio e dell'ulna sono stati utilizzati i metodi di segmentazione "Thresholding" e "RegionGrowing" sulle immagini e grazie ad operatori morfologici, è stato possibile distinguere l'osso corticale dall'osso spongioso. Successivamente è stata creata la cartilagine presente tra le due ossa, attraverso operazioni di tipo booleano. Invece, i legamenti sono stati realizzati prendendo i punti-nodo del radio e dell'ulna e formando le superfici tra di essi. Per ciascuna di queste componenti, sono state assegnate le corrispondenti proprietà dei materiali.

Per migliorare la qualità dei modelli, sono state necessarie operazioni di "Smoothing" e "Autoremesh".

In seguito, è stata eseguita un'analisi agli elementi finiti attraverso l'uso di vincoli e forze, così da simulare il comportamento delle articolazioni. In particolare, sono stati simulati lo stress e la deformazione.

Infine, grazie ai risultati ottenuti dalle simulazioni, è stato possibile verificare l'eventuale rischio di frattura in differenti punti anatomici del radio e dell'ulna nell'articolazione sana e patologica.

# 1. Introduction

## 1.1 Anatomy and Function

The complex movements allowed to hand are the result of more movable joints that establish between the bones which make up the same hand. There are 27 bones in the hand in all, divided between the carpal bones (8) of the metacarpal (5) and the phalanges of the fingers (14).

The joints of the hand are:

- Wrist joints
- Carpal joints
- Metacarpal joints
- Fingers Joints

There are six distinct joint cavities which follow, from the wrist to the metacarpal: distal radio-ulnar, radio-carpal, piso-pyramidal, mid-carpal, medial carpo-metacarpal and lateral carpo-metacarpal joint

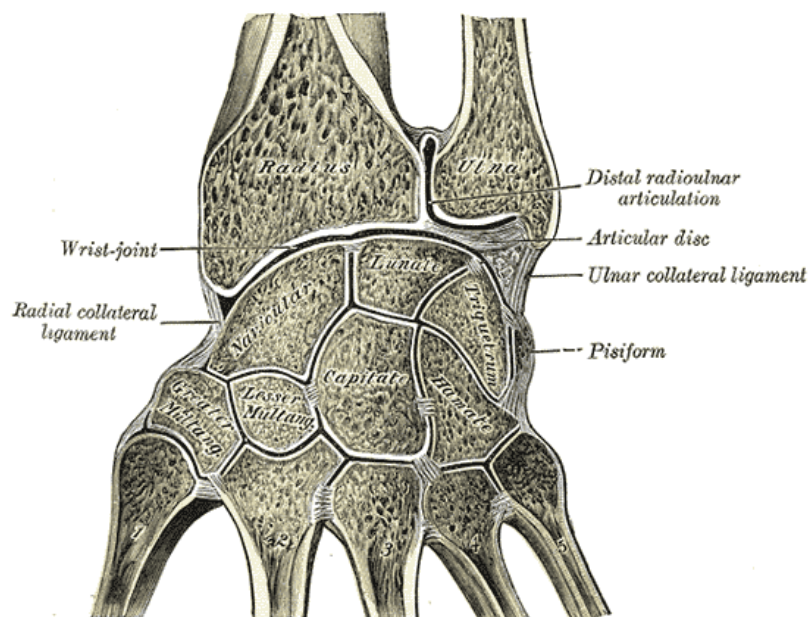


Figure 1 - Frontal section of the wrist and carpus joints

The radio-ulnar joint (DRUJ) is the articulation of the upper limb, located in the forearm, which connects ulna and radius. The movements that can be exercised on it are pronation and supination of the forearm. Ulna and radius are connected via two mobile joints, the proximal and distal radio-ulnar joint, and a semi-mobile interosseous membrane



Figure 2. Proximal and distal radio-ulnar joint

Two intrinsic ligaments reinforce the joint:

- Palmar radio-ulnar ligament, that originates from the anterior margin of the radius and ulnar incisura and it is part of the anterior margin of the radial articular ulna facet
- Dorsal radio-ulnar ligament, that originates from the posterior margin of the radius and ulnar incisura and it is part of the posterior margin of the radial articular ulna facet.

The distal radio-ulnar joint plays an important role in forearm rotation and positioning of the hand for activities of daily living [2].

Stability of this joint is a result of contributions from both its osseous anatomy and the soft tissues surrounding the joint [3-7].



Instability typically follows because osseous damage, ligamentous damage, or both occur. Therefore soft tissue constraints, both active and passive, are crucial to the stability and function of the joint.

There is currently a limited understanding of distal radio-ulnar joint kinematics. The curvature of the sigmoid notch of the radius is, on average, approximately 50% greater than the ulnar head with which it articulates [7,8]. This relatively incongruous bony articulation between the sigmoid notch of the radius and the ulnar head allows for noteworthy translation in addition to rotation but does not lend itself to stability of the joint [9].

The distal radio-ulnar joint is an intricate part of wrist function. The radius and hand move in relation to, and function about, the distal ulna. The anatomic relations between the distal radius and ulna and the ulnar carpus are precise, and even minor modifications in these relations leads to significant load-pattern changes.

In this complicated apparatus, the ulnar head forms the pivotal point in relation to which the normal position of other bony landmarks are determined and about which all motions of the wrist are believed to occur [10].

Recently, it is appreciated that the DRUJ has an important role in distributing the applied load through the osseoligamentous system [11,12]. In this system, the interosseous ligament (IOL: central band of the interosseous membrane) plays an important role; it is a strong ligament that connects the radius and ulna in the mid-forearm. Compression of the forearm is a mode of loading which causes tension to develop in the IOL and in traumatic conditions may cause clinical problems such as radial head fracture and injury to the IOL [13].

The integrity of the osseoligamentous system is vital to normal function of forearm and the removal of one and even part of one of the 2 bones from the forearm can disrupt the functional integrity of this linked system, leading to weakness of grip strength and inability to lift heavy loads [14]. The disruption of radio-ulnar ligaments (DRUL) alone notably disrupts joint biomechanics [15].

## 1.2 Segmentation methods, Morphologic and Boolean Operations

*Segmentation* splits the image into non-overlapping regions that fulfill a certain criteria of belonging; these regions have to satisfy some properties:

- *distinct*, no pixel is shared by two regions;
- *complete*, all pixels are assigned to at least one region;
- *connected*, all pixels belonging to the region are “connected”;
- *homogeneous*, all regions are homogeneous with respect to a fixed criterion.

There are pixel-based, region-based and edge-based methods. In this work, two methods of Segmentation were used: “Thresholding” and “Region Growing”.

*Thresholding* is a pixel-based method on which each pixel is segmented according to its value of gray level (histogram). In particular, individual pixels of the image are cataloged as "pixel object" if their value is greater than a certain threshold, and as "pixel background " if the value is below the threshold [16]. *Region Growing* is a simple region-based method. It is also classified as a pixel-based image segmentation method since it involves the selection of initial seed points. This approach to segmentation examines neighboring pixels of initial “seed points” and determines whether the pixel neighbors should be added to the region.

The *Binary Morphologic Operators* are operators between sets defined on the basis of the binary image.

The binary image is seen as a subset of the 2D set of integers ( $E^2$ ).

The Union of two sets is the set of all elements that belong to A or B or either:

$$C = A \cup B$$

The Intersection of two sets is the set of all elements that belong to A or B:

$$D = A \cap B$$

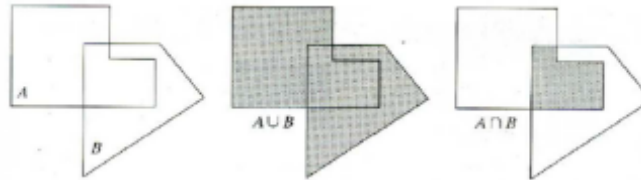


Figure 3. Example of Union and Intersection operations

The Difference of two sets A and B (A-B) is defined as:

$$A - B = \{w | w \in A, w \notin B\} = A \cap B^c$$

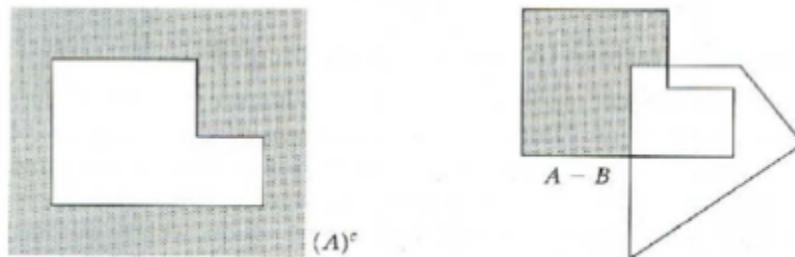


Figure 4. Difference operation

The Boolean Operations on binary images are:

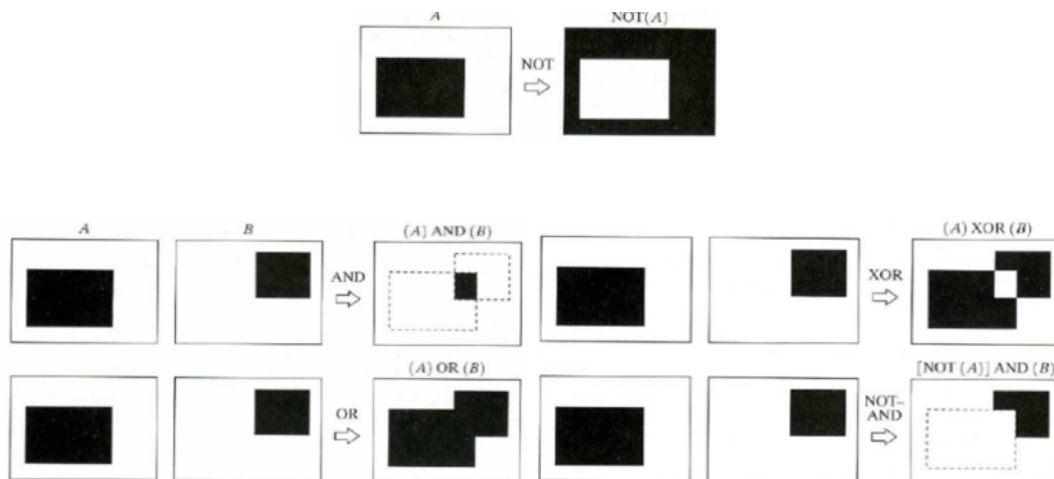


Figure 5. Examples of Boolean Operations

*Erosion* and *Dilation* are the most basic operators of the mathematical morphology

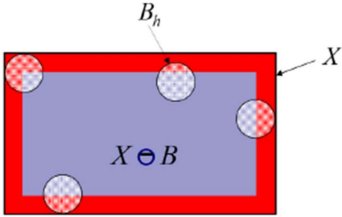
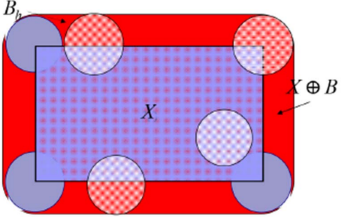
Erosion	Dilation
$(X) = X \ominus B = \{h   B_h \subseteq X\}$	$X \oplus B = \{h   Bh \cap X \neq \emptyset\}$
	

Table 1. Most basic operators of the mathematical morphology

More complex morphologic operators can be defined as a combination of Erosion and Dilation [17-26] .

### 1.3 Finite Element Model

In mathematics, the *Finite Element Method* (FEM) is a numerical technique for finding approximate solutions to boundary value problems for differential equations. It uses variational methods (the calculus of variations) to minimize an error function and produce a stable solution. Analogous to the idea that connecting many tiny straight lines can approximate a larger circle, FEM encompasses all the methods for connecting many simple element equations over many small subdomains, named finite elements, to approximate a more complex equation over a larger domain.

The main characteristic of the Finite Element Method is the discretization through the creation of a grid (mesh) composed of primitives (finite elements) of coded form (triangles and quadrilaterals for 2D domains, hexahedral and tetrahedral domains for 3D)

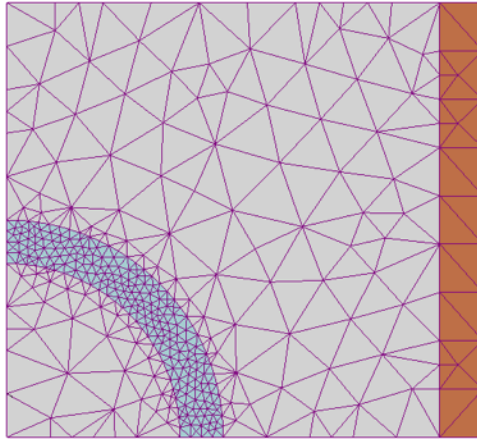


Figure 6. FEM mesh created by an analyst prior to finding a solution to a magnetic problem using FEM software. Colors indicate that the analyst as set material properties for each zone, in this case a conducting wire coil in orange; a ferromagnetic component in light blue; and air in grey. Although the geometry may seem simple, it would be very challenging to calculate the magnetic field for this setup without FEM software, using equations alone

On each element characterized by this elementary form, the solution of the problem is expressed by the linear combination of functions called shape functions. Note that at times the function is approximated, and not necessarily the exact values of the function will be those calculated in the points, but the values that will provide the least error across the entire solution .

The subdivision of a whole domain into simpler parts has several advantages [27]:

- Accurate representation of complex geometry
- Inclusion of dissimilar material properties
- Easy representation of the total solution
- Capture of local effects.

A typical work out of the method involves dividing the domain of the problem into a collection of subdomains, with each subdomain represented by a set of element equations to the original problem, followed by systematically recombining all sets of element equations into a global system of equations

for the final calculation. The global system of equations has known solution techniques, and can be calculated from the initial values of the original problem to obtain a numerical answer.

In the first step above, the element equations are simple equations that locally approximate the original complex equations to be studied, where the original equations are often partial differential equations (PDE). To explain the approximation in this process, FEM is commonly introduced as a special case of Galerkin method. The process, in mathematics language, is to construct an integral of the inner product of the residual and the weight functions and set the integral to zero. In simple terms, it is a procedure that minimizes the error of approximation by fitting trial functions into the PDE. The residual is the error caused by the trial functions, and the weight functions are polynomial approximation functions that project the residual. The process eliminates all the spatial derivatives from the PDE, thus approximating the PDE locally with:

- a set of algebraic equations for steady state problems
- a set of ordinary differential equations for transient problems

These equation sets are the element equations. They are linear if the underlying PDE is linear, and vice versa. Algebraic equation sets that arise in the steady state problems are solved using numerical linear algebra methods, while ordinary differential equation sets that arise in the transient problems are solved by numerical integration using standard techniques such as Euler's method or the Runge-Kutta method.

A global system of equations is generated from the element equations through a transformation of coordinates from the subdomains' local nodes to the domain's global nodes. This spatial transformation includes appropriate orientation adjustments as applied in relation to the reference coordinate system. The process is often carried out by FEM software using coordinate data generated from the subdomains. FEM is best understood from its practical application, known as finite element analysis (FEA). FEA as applied in engineering is a computational tool for performing engineering analysis. It includes the use of mesh

generation techniques for dividing a complex problem into small elements, as well as the use of software program coded with FEM algorithm.

To arrive at the final Finite Element Model follow the fundamental phases, each of which involves the propagation of errors in the final solution:

1. *Modeling*: it is possible to pass from the physical system to a mathematical model that abstracts some aspects of the physical system of interest, focusing on a few aggregate variables of interest and "filtering out" the remaining. If the physical system is complex, it is possible to divided it into subsystems. Il sistema fisico se complesso viene suddiviso in sottosistemi; The subsystem will then be divided into finite elements to which is applied a mathematical model. Unlike analytical treatments, it is sufficient that the mathematical model is appropriate to the simple geometry of finite elements. The choice of a type of element in a software program is equivalent to an implicit choice of the mathematical model that is the basis.
2. *Discretization*: in a numerical simulation, it is necessary to switch from an infinite number of degrees of freedom (the condition of "continuum") to a finite number. The discretization, in space or in time, has the aim to obtain a discrete model characterized by a finite number of freedom degrees.

FE models, when compared with most experimental techniques, offer the advantage of estimating the stress/strain field over the whole region of interest rather than in a few selected points, and permit a time-effective and virtually infinite variation of study parameters. Moreover, image processing and FE model generation procedures developed in the last 20 years (Keyak et al. 1990; Lotz et al. 1991; Viceconti et al. 2004; Taddei et al. 2007) facilitate patient-specific FE models to be derived from in vivo diagnostic data, while the mechanical stress in bones cannot be measured in vivo without the use of an invasive, and in most cases unethical, surgical procedure (Aamodt et al. 1997). Subject-specific modelling procedures (see Viceconti & Taddei (2003) for a review on this topic) enable the creation of an FE model of a bone segment from computed tomography (CT) images.

Such procedures currently represent the best source of information on long bone morphology and mechanical properties applicable in vivo. As a result of the continuous technical improvements in image processing and the widespread use of CT imaging, the number of subject-specific FE modelling studies is exponentially growing, exceeding 100 papers in the biomechanics literature (Schileo et al. 2008b) [28].

The finite element method has been employed with considerable success to explore load distribution and deformation patterns at a variety of locations in the human body. The application of the method has been particularly successful in joints with relatively simple geometry and well defined loading conditions, such as the hip [29,30]. The development of an understanding of the etiology of pathology and the ability to predict the consequences of surgical intervention have been possible using these methods. The finite element method has had less impact on knowledge of the mechanics of multi-bone joints such as the wrist [31].

The wrist poses a challenge in biomechanical modeling due to the complex interactions between the many bones comprising the joint. Each bone will contribute uniquely to the high range of motion of the joint. The challenge in modeling of the multibone models is to capture the mechanism contributing to the stabilization of the joint. A stable joint is able to provide three-dimensional equilibrium under external loading which can also be interpreted as the ability of a joint to maintain a normal relationship between the articulating bones and soft tissue constraints under physiologic loads throughout the whole range of motion [32]. This implies that the joints need to be capable of distributing loads without generating abnormally high stresses on the articulating surface as well as being able to move within the joint's range of motion. Geometry of the bones also plays an important role in joint stability and the concavity or convexity of the articulating bones helps the bones to distribute stresses across the joint [33].

Only a small number of studies have presented analysis of the load transfer through the wrist. For example, Nedoma et al. [34] and Schuind et al. [35] present studies using simplified representations of the joint structures. The finite element method has been applied, but again due to the complexity of the articulations, geometrical simplification of the joint and its structures has been used. In 1995, Anderson and Daniel [36] created a plane strain model



of the radio-carpal joint which consisted of the radius, scaphoid and the lunate. This was one of the first attempts to address the loading on the radiocarpal joint using finite element methods. Two-dimensional modeling was used throughout. The output from 2D models offers some insight into load transfer, but must be treated with caution.

In 2009 full three dimensional models of the wrist were published by Gislason et al [37] and Guo et al [38] incorporating the distal ends of the radius and ulna, all the carpal bones as well as the metacarpals. The Gislason model aimed to simulate load transfer behavior of the wrist during gripping in three different subjects with the wrist in three different positions. The loading was determined on a subject specific basis where the forces and moments acting on the fingers were measured and by using a biomechanical model, the external forces were converted into joint contact forces acting on the metacarpals. The Guo model aimed to simulate the carpal bone behavior after the transverse carpal ligament had been excised. The loading applied onto the Guo model was a combined 100 N compressive force acting on the the 2<sup>nd</sup> and 3<sup>rd</sup> metacarpal and some unphysiological constraints were applied to the model

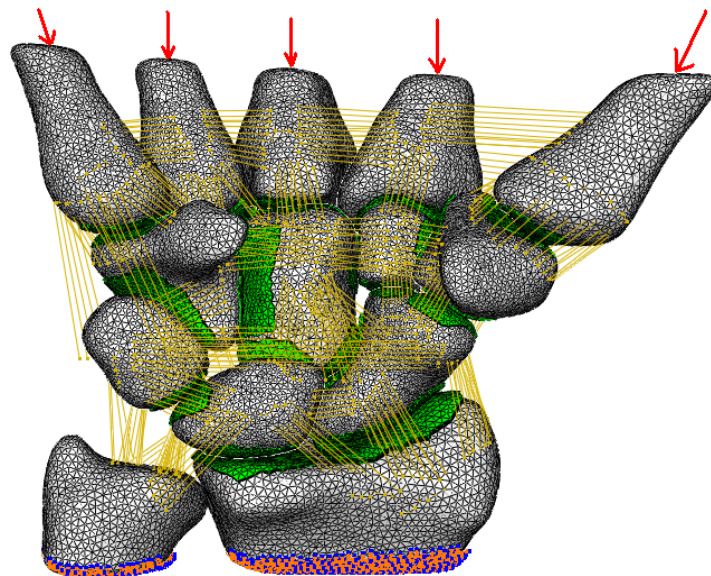


Figure 7. Finite Element Model of Gislason et al. [37]

## 1.4 Aim

This thesis will concentrate on the development of Finite Element Modeling Methods in the distal radio-ulnar joint.

Two 3D models will be designed from DICOM CT-images. Images belonged to a patient with healthy joint and a patient with pathologic joint; in particular, the pathology is caused by a traumatic dislocation of the ulna.

The model will be developed in order to understand the issues of bone geometry and interaction, constraints and contact modeling, mesh refinement and in addition physiologically reasonable loading will be applied at the boundaries. After the simulations of the model, it will be possible to assess the possible risk of fracture in different anatomical points of bones that compose the DRUJ.

## **2. Material and Methods**

### **2.1 Defining the geometry**

The geometrical representation of models was obtained by CT scans. The scans were taken of wrists belonged to a patient with healthy joint and a patient with pathologic joint. The images ranged from the distal end of the two forearm bones, radius and ulna, to the proximal third of the metacarpals. The CT images were imported into “Mimics”, in DICOM format.

“Mimics” is a software for medical image processing, in particularly for the segmentation of 3D medical images and the result will be highly accurate 3D models of the patient’s anatomy [39].

#### **2.1.1 Radius and Ulna Bones**

To create the *Radius* and *Ulna* bones, it was necessary to use methods of Segmentation. The Segmentation was carried out in the axial plane, that it was the plane with the highest resolution; in order to obtain a refined Segmentation and then a full 3D representation, it was possible to use the sagittal and coronal plane, with a lower resolution.

The first step was to detect the edge of all bone tissue, through “Thresholding”, which involved masking out each pixel belonging to each bone within a given slice.

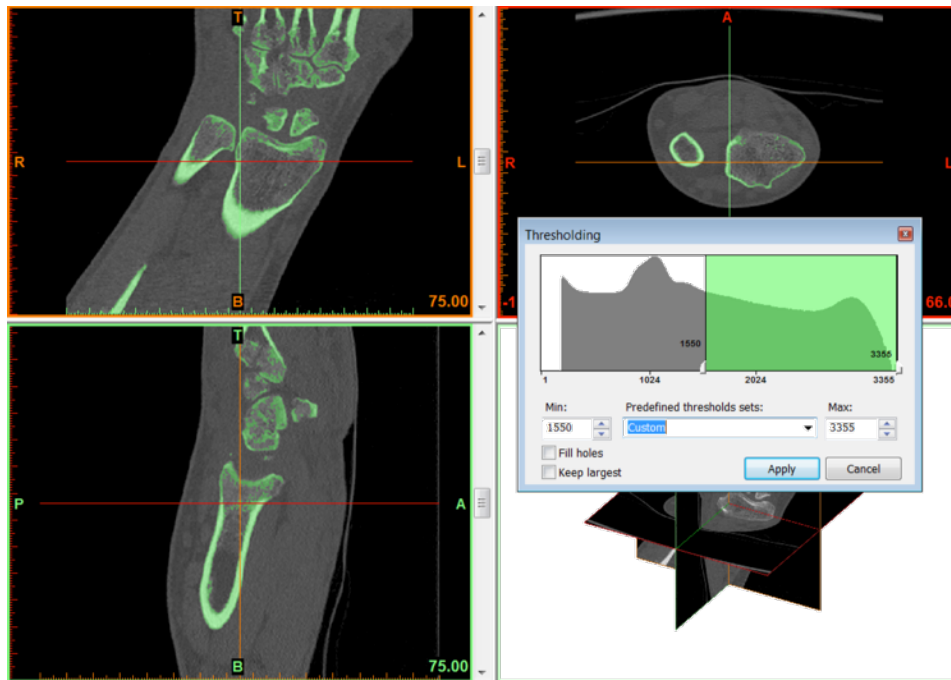


Figure 8. Threshold to detect the bone tissue

At this point, the goal was to create the masks of two bones of interest and it was necessary to select before the edge of radius bone and subsequently the edge of the ulna bone. To do this, it was used the “RegionGrowing”. In this work, to select a set of seed points, it was necessary to click on one of points of the radius (Figure 9) and then of the ulna

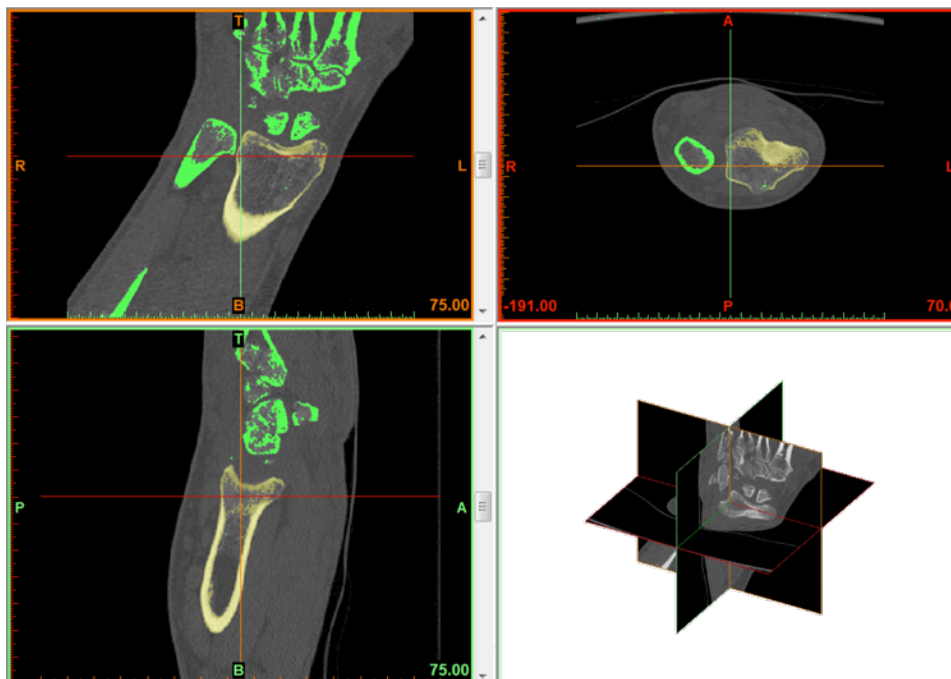


Figure 9. The cross represents the Radius seed point used for Region Growing

The next step was to get, in all three views, the contour and area of the radius and ulna well defined in each slice. To facilitate the work of drawing and filling, two tools of “Mimics” were used: one of these added pixels to the mask of interest and the other one calculated in the axial view, a new set of polylines, that created contours which included all the edited area

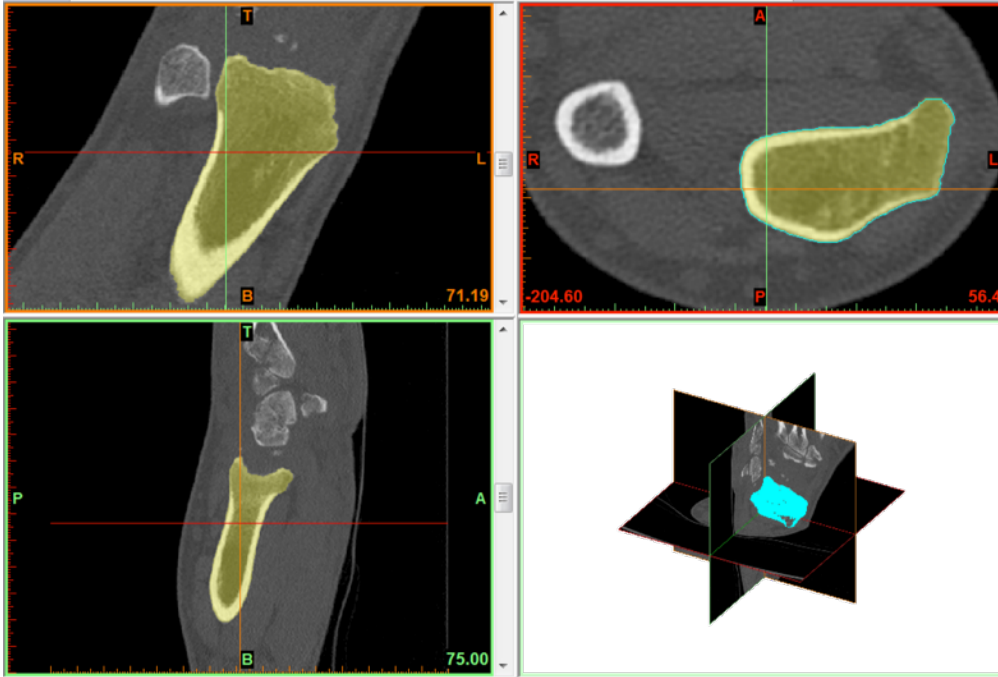


Figure 10. Set of polylines used to create the contour of Radius; the same step was useful to create Ulna contour

Finally, the masks of Radius and Ulna were obtained

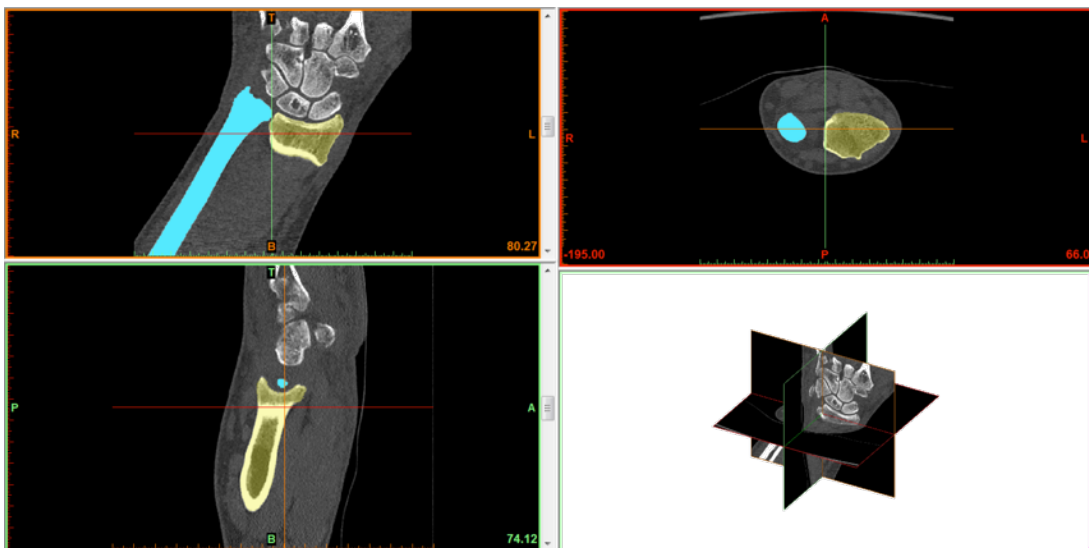


Figure 11. Cyan mask represented the Ulna bone; yellow mask represented the Radius bone

After creating the masks of Radius and Ulna bones, it was necessary to use the Morphologic and Boolean Operators to distinguish the *Cortical* and the *Cancellous Bones*.

Two masks were created: one of them (red or pink mask in the Figure 12) represented the cortical part of the bone and the other one (orange or cyano mask in the Figure 12) represented the cancellous part of the bone.

At the first moment, it was possible to use the Morphologic Operations that allowed to create the cancellous bone; particularly, to do this, the Erode Operation was used.

Subsequently, to create the masks of cortical bone, it was used “XOR”, a Boolean Operation between mask of whole bone and the mask of cancellous bone

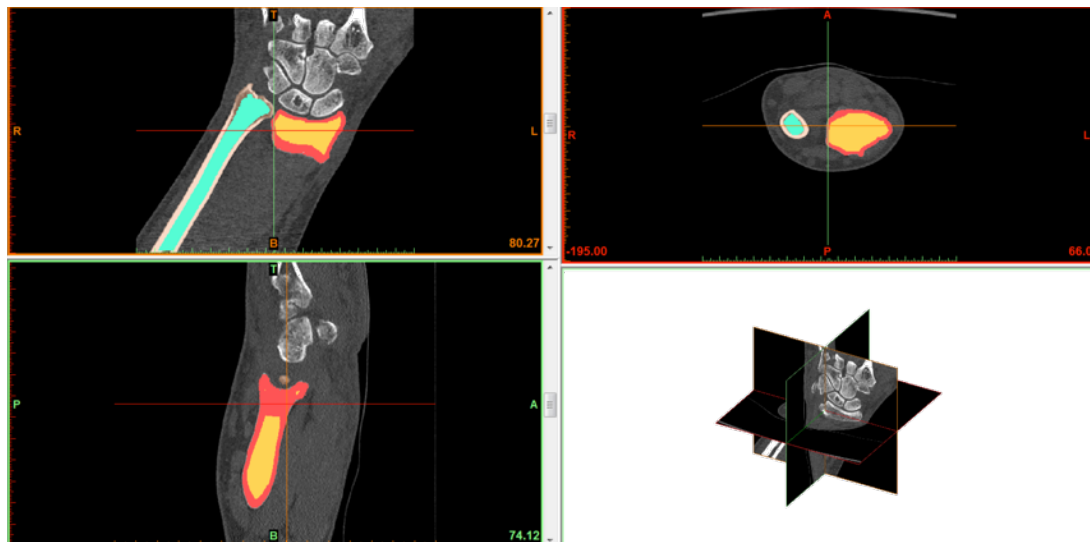


Figure 12. Pink and red masks represented respectively the Ulna and Radius Cortical bone; cyan and orange masks represented respectively the Ulna and Radius Cancellous bone

All these steps, described so far, were used for the realization of the Radius and Ulna for both models (healthy and pathological).

## 2.1.2 Cartilage

Not having available MRI images of the two joints, a strategy was used to obtain an approximate model of representation of Cartilage as similar as possible to the anatomical Cartilage

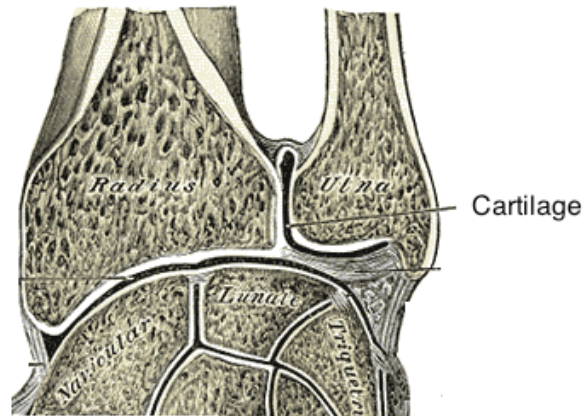


Figure 13. Anatomical cartilage between Radius and Ulna

The strategy followed these steps:

- Creation of a green mask between the masks of the Radius and Ulna

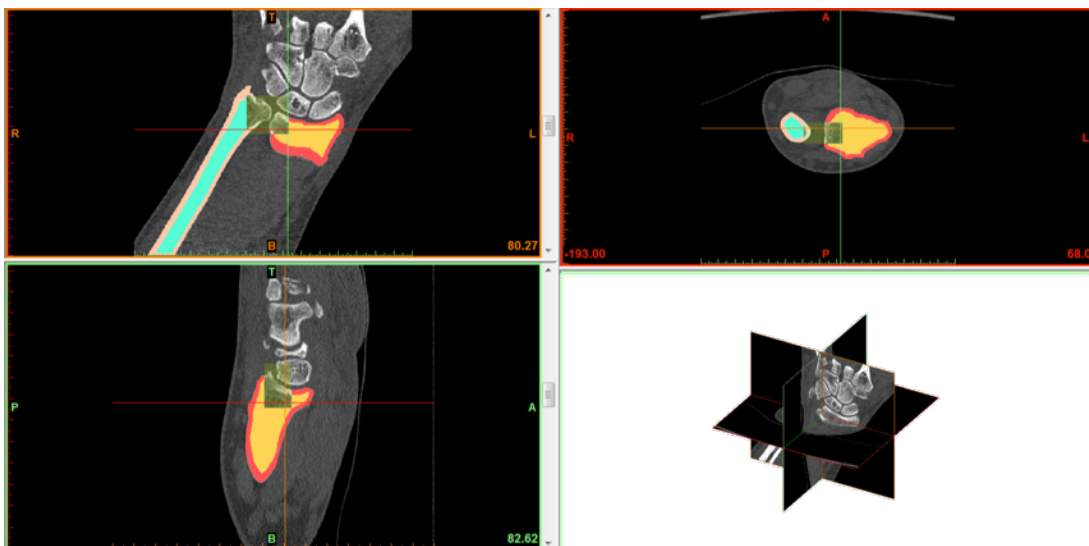


Figure 14. First step to realize the Cartilage Mask

- With the Boolean Operation, known in “Mimics” as “minus”, between the green and Ulna masks, the purple mask was obtained

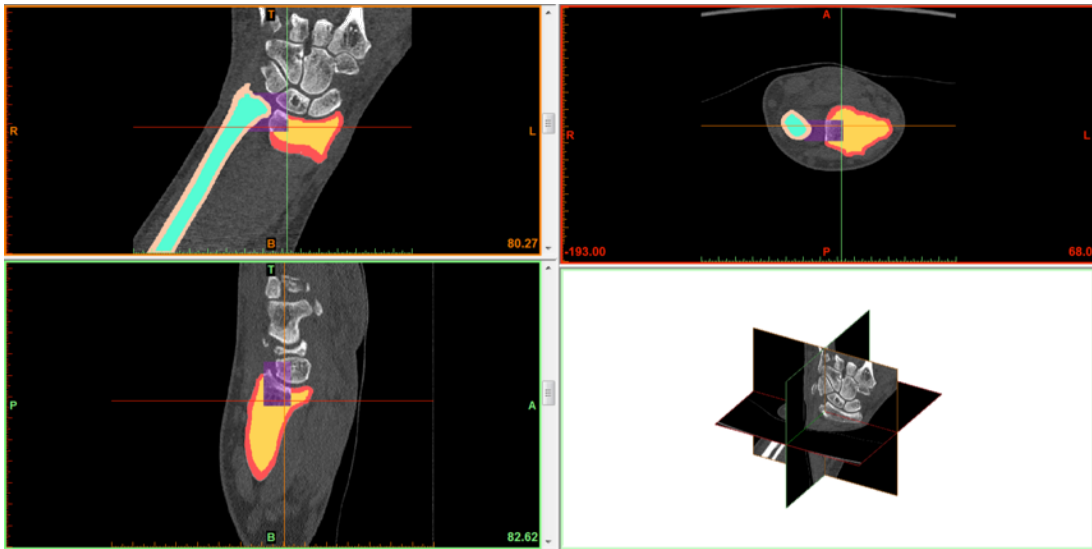


Figure 15. Second step to obtain the Cartilage Mask

- Then, the Boolean Operation “minus” was applied another time, between the purple and Radius mask

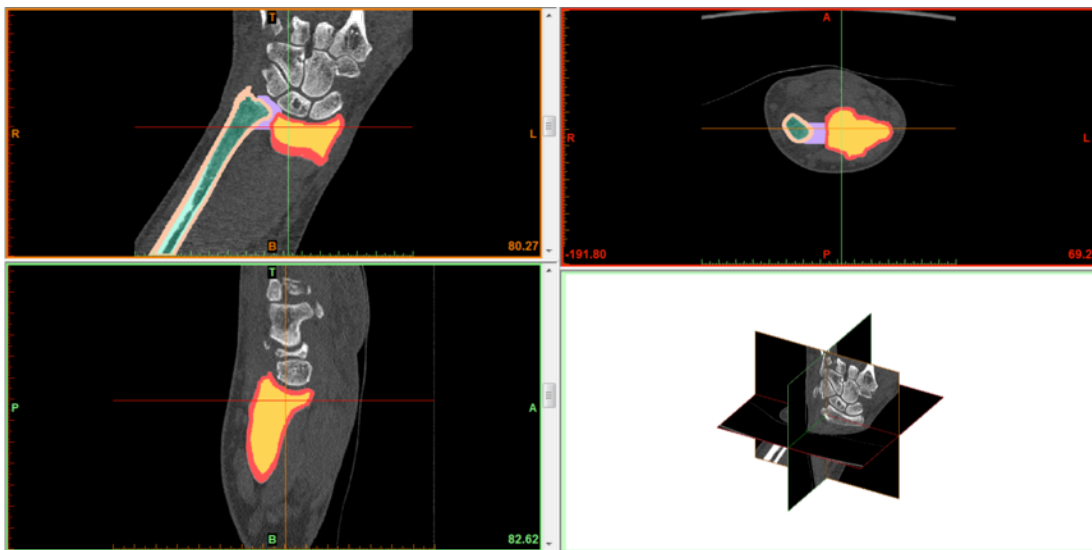


Figure 16. Last step to realize the Cartilage Mask

The violet mask represented the mask of Cartilage.



## 2.2 Meshing the cartilage and bones

After creating the masks of bones, they were reconstructed into a three-dimensional objects

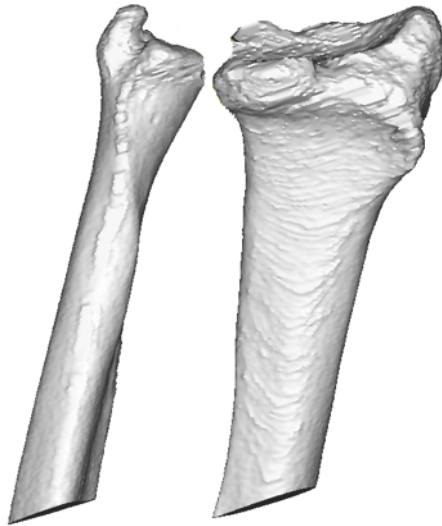


Figure 17. Raw 3D object of Radius and Ulna

Then, the 3D Model of the cartilage mask was created

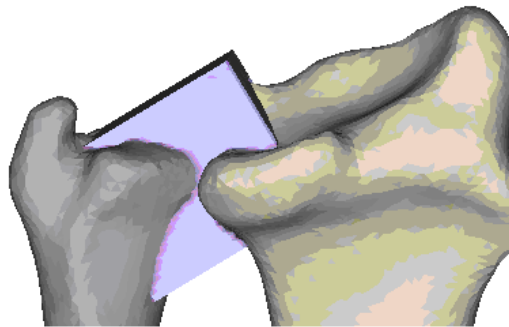


Figure 18. Cartilage 3D object realized starting to purple mask (see section 2.2)

To model this object and make it as much as possible similar to the anatomical cartilage (Figure 13), a tool of Mimics was used to modify the 3D object

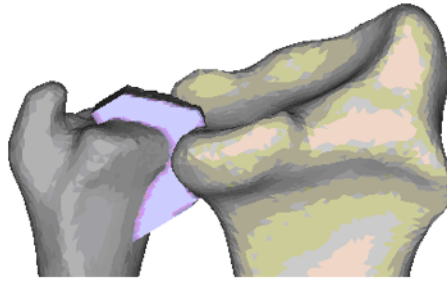


Figure 19. Cartilage 3D object, as much as possible similar to the anatomical Cartilage

Right at the phase of creation of the cartilage 3D model in the pathological joint, that it was possible to observe the dislocation of the ulna with respect to its anatomical position

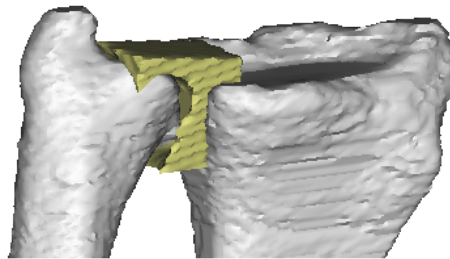


Figure 20. Ulna dislocation in the pathological model

After the creation of geometrical objects, they were meshed using a semi-automatic mesher incorporated in Mimics, called “3-Matic”.

“3-Matic” is able to combine CAD tools with pre-processing (meshing) capabilities. To do this, it works on triangulated (STL) files and as such, it is suitable for organic/freeform 3D data such as the anatomical data resulting from the segmentation of medical images (from Mimics) [40].

In this work, the surfaces were meshed using triangular surface elements.

To improve the quality of two models realized in the previous steps, it was necessary to apply operations of “Smoothing” and “Remesh”. These operations are tools of the “3matic” software and were able to optimize the triangles shape, making equilateral, homogeneous and better defined

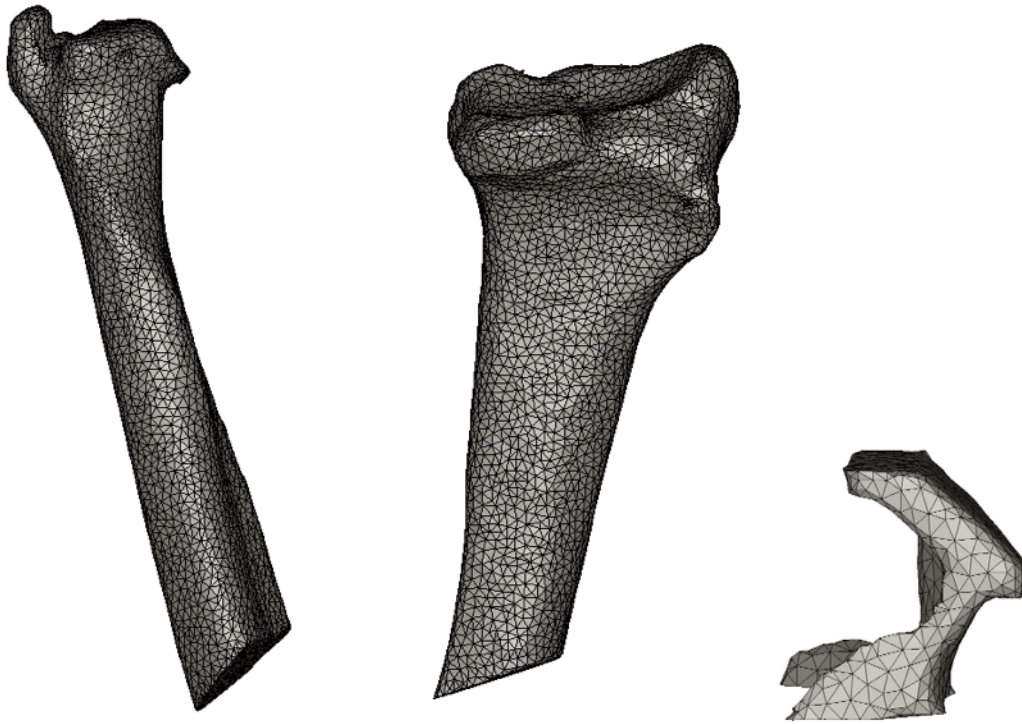


Figure 21. Ulna, Radius and Cartilage meshes after “Smoothing” and “Remesh”

The finite element model was built up by converting the surface meshes into tetrahedral elements.

## 2.3 Ligaments

In this model, three types of ligaments were incorporated: interosseous, dorsal and palmar. To create them, a software called “*SolidWorks*” was used. The *ligaments* were created by taking the node-points of the radius and ulna, a spine was created through them and then the area of the ligaments was generated automatically from the software starting to node points

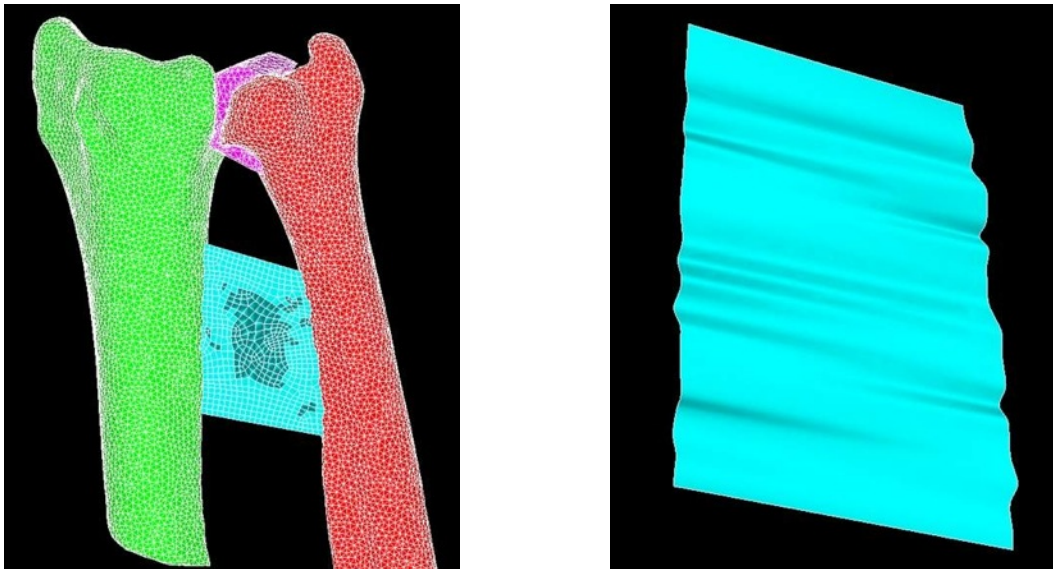


Figure 22. Interosseous ligament

In particularly, at the distal end of the radius /ulna, there is a dorsal ligament that forms some sort of triangle, but it is difficult to create the ligament without intersecting the surface of the bone. As shown in the following figure of the dorsal ligament, then it does intersect a bit, but we can live with that

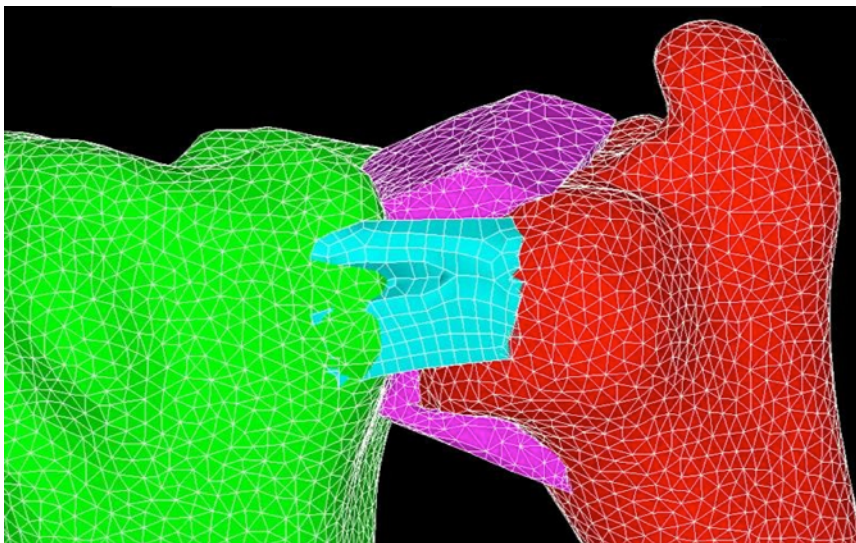


Figure 23. Dorsal ligament

Finally, the palmar ligament was created

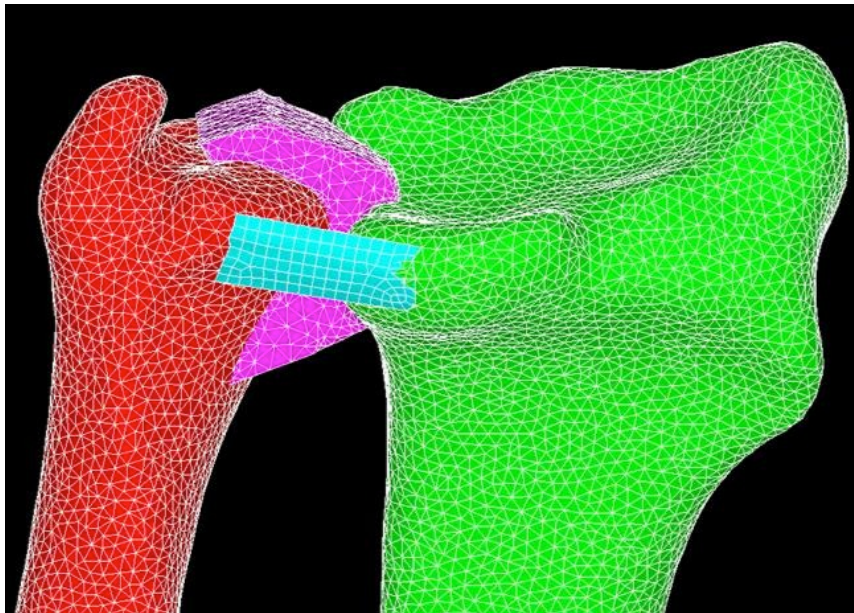


Figure 24. Palmar ligament

These ligaments were exported in a STL format from “SolidWorks” to “Mimics”, where they were repositioned properly.

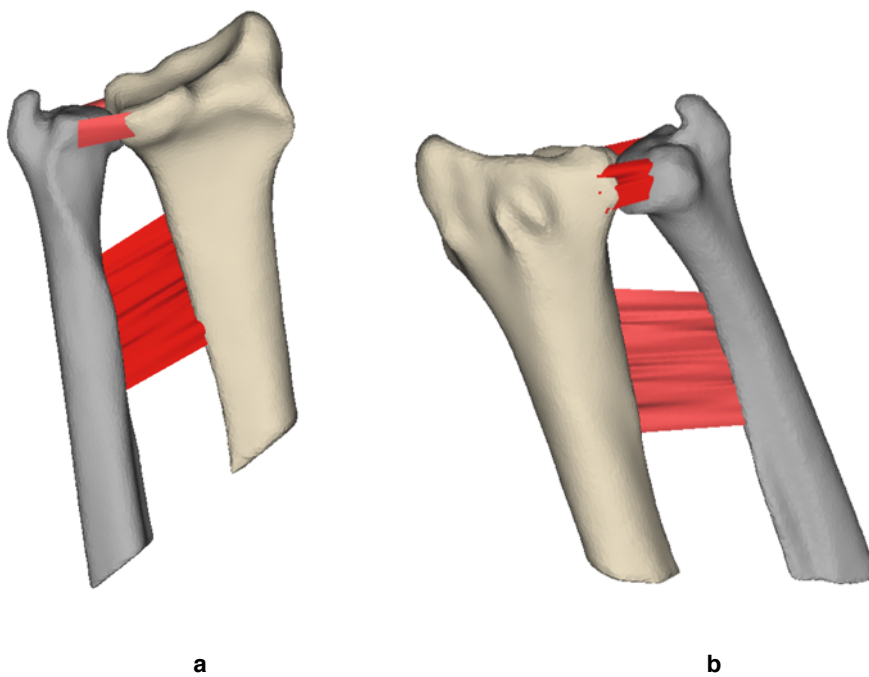


Figure 25. a) Palmar and Interosseous ligaments; b) Dorsal and Interosseous ligaments

## 2.4 Tissue properties Modeling

At this point, two models needed to material properties of radius, ulna and cartilage.

“Mimics” assigned materials to volumetric meshes based on Hounsfield gray values. After creating a volume mesh in the remesher “3-matic”, the volume mesh take back into “Mimics” and then the material properties were assigned.

It was necessary to set in Mimics the value of the E-modulus and Poisson Coefficient.

In particular, the *E-modulus* is the Young modulus that describes the tensile elasticity, or the tendency of an object to deform along an axis when opposing forces are applied along that axis; it is defined as the ratio of tensile stress to tensile strain [41,42]

$$E = \frac{stress}{strain}$$

Assuming that the material is stretched or compressed along the axial direction (the x axis in the below diagram), the Poisson’s ratio is:

$$\nu = - \frac{d\varepsilon_{trans}}{d\varepsilon_{axial}} = - \frac{d\varepsilon_y}{d\varepsilon_x} = - \frac{d\varepsilon_z}{d\varepsilon_x}$$

The cartilage and bones were modeled using linear, isotropic material properties. For the cortical and cancellous bones were used the Young’s modulus of 18 GPa and 100 MPa respectively [31]. The range of values in the literature for the Young’s modulus of bone is great. Nearly all finite element studies carried out on joint mechanics have modeled bone as a linear isotropic material. The Poisson’s ratio values used for the radius were 0.25 for cortical bone and 0.35 for cancellous bone. For the ulna, the Poisson’s ratio values were 0.2 for cortical bone and 0.3 for cancellous bone. The cartilage was modeled using a Young’s modulus of 10 MPa and the Poisson’s ratio values was 0.45.

The material properties of ligaments will be assign later in the finite element solver “Ansys Workbench”, because in “Mimics” it is not possible to assign the materials at the STL files.

## 2.5 Finite Element Analysis

All programs that use the Finite Element Method for structural analysis are equipped with a library of one-dimensional, two-dimensional and three-dimensional finite element in order to facilitate the modeling of a real structure [44-51].

In this work, the model was solved using Ansys Workbench. The singol component of two models were exported in Ansys format. For the radius, ulna and cartilage that have the material properties, two files were obtained, one of these was in the .cdb and the other was in .txt (it contained the information about the material properties). For the ligaments, the STL model of every single ligament was opened in “3-matic” and then, each ligament was exported in Ansys format, obtaining three files .cdb.

Initially, the .cdb files of the components were uploaded in Workbench and a “Initial Geometry” (FEM, Finite Element Modeler) was calculated

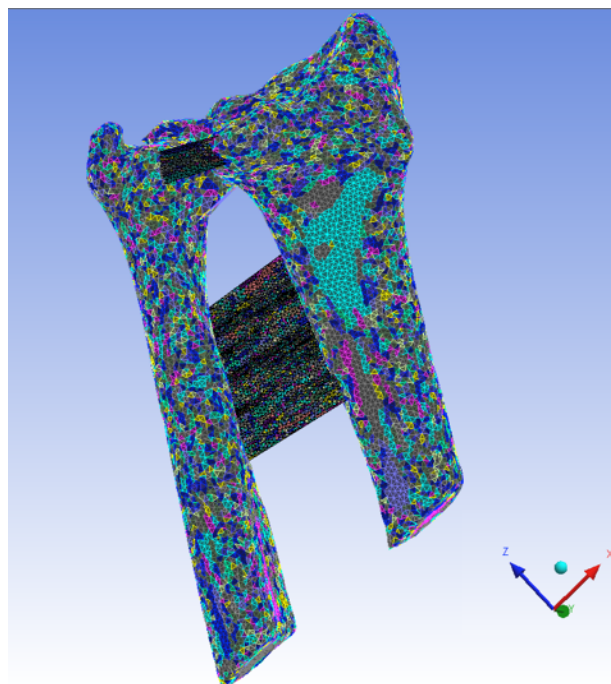


Figure 26. Initial Geometry of the Model calculated through FEM

To calculate the “Initial Geometry”, a tolerance angle (see Figure 27) was used to divide the surface into triangle areas. On these triangles, it was possible to apply forces and supports etc. In this simulation, to be able to accurately apply forces and supports, after some tests, it was seen that an angle equal 1 should do the trick,

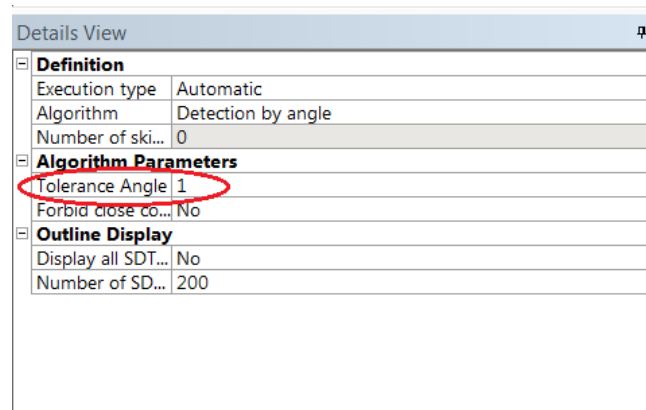


Figure 27. Tolerance angle used to divide the surface into triangle areas

It was necessary to upload the material properties of components and to create the material properties of ligaments

Properties of Outline Row 4: ligaments			
	A	B	C
1	Property	Value	Unit
2	Density	1,001E+11	kg m <sup>-3</sup>
3	Isotropic Elasticity		
4	Derive from	Young's Modulus...	
5	Young's Modulus	10	MPa
6	Poisson's Ratio	0,4	
7	Bulk Modulus	1,6667E+07	Pa
8	Shear Modulus	3,5714E+06	Pa

Figure 28. Ligaments material properties



After the updating, a surface-to-surface contact was established between the articulating surfaces

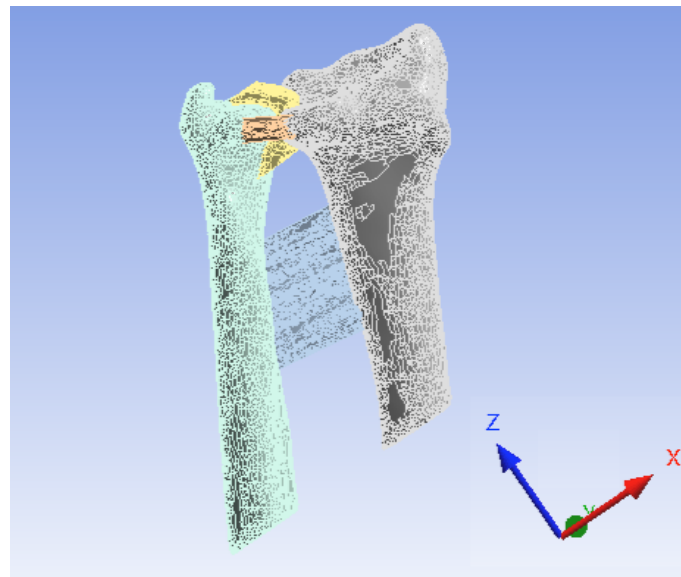


Figure 29. Static Structural of Model

## 2.5.1 Model Constrains

The model needed to be fixed somewhere to make simulation possible without non-physiological movements. The proximal ends of the radius and ulna were fully constrained and not allowed to translate or rotate

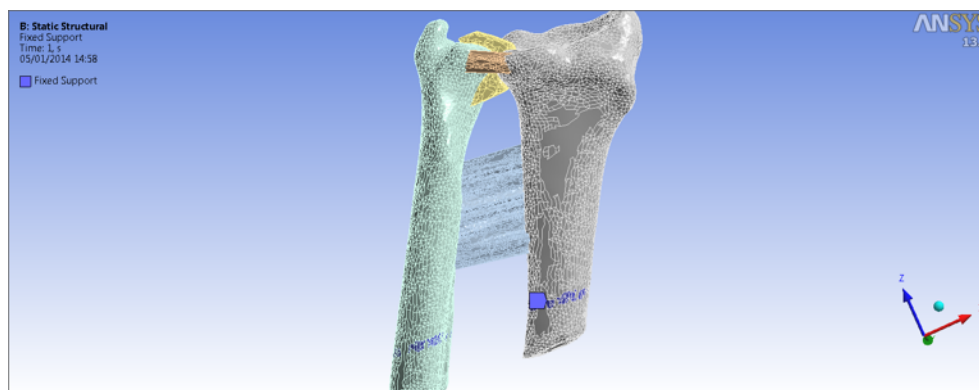


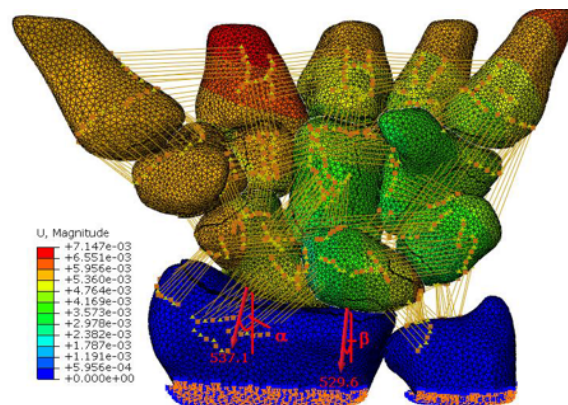
Figure 30. Model with fixed support

## 2.5.2 Specification of loading conditions

The aim of this work was to simulate the movement of “twist” of the joints, under the “radioscaphoid” and “radiolunate” forces.

The loading conditions were chosen starting from the previous study [52], where four types of modelling conditions were analysed:

1. Untreated wrist
2. Radiolunate fusion
3. Radioscaphoid fusion
4. Radiolunate and Radioscaphoid fusion



Condition	RS [N]	RL [N]	$\alpha$ [°]	$\beta$ [°]
1	537.1	529.6	15.3	6.8
2	403.8	418.7	18.3	-37.7
3	547.0	439.2	-29.7	2.9
4	569.0	358.1	-29.4	-19.2

a

b

Figure 31. a) Displacement plot for the untreated wrist with reaction forces acting on the radioscaphoid and radio-lunate joints. Magnitude and direction of the joint reaction forces are illustrated with red arrows; b) The magnitude and angle of the reaction forces acting on the radiocarpal joints for the four conditions [52].

According with the study of healthy wrist model mentioned above, it was chosen a physiological “radioscaphoid” force equal to 540 N under a 15° in the frontal panel on the radioscaphoid articulation. To apply this force, it was necessary to set the x, y, z components of the force and they were calculated



$$F = 540 \text{ N}$$

$$\alpha = 15^\circ$$

$$F_x = F \sin \alpha = 139.7$$

$$F_z = F \cos \alpha = 521.6 \text{ N}$$

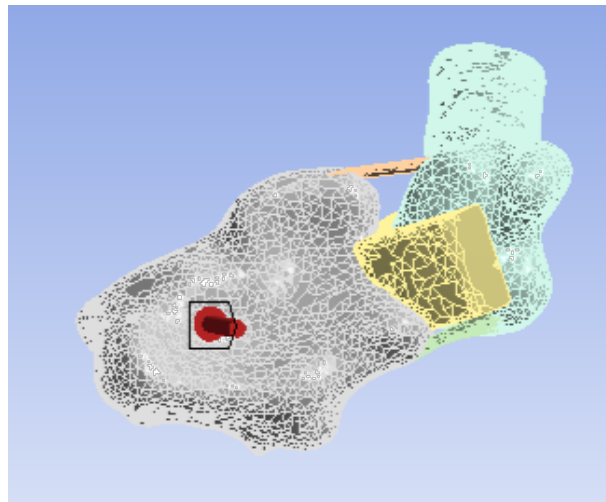


Figure 32. Force on the radioscaphoid articulation

It was chosen a “radiolunate” physiological force equal to 520 N under a 4° in the frontal panel on the radiolunate articulation. Also in this case, the x, y, z components of the force were calculated



$$F = 520 \text{ N} \quad F_x = F \sin \alpha = 36.3 \text{ N}$$

$$\alpha = 4^\circ \quad F_z = F \cos \alpha = 518.7 \text{ N}$$

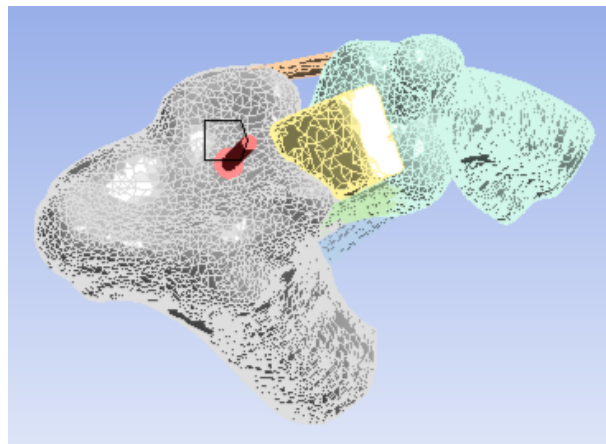


Figure 33. Force on the radiolunate articulation

To simulate the movement of “twist” under the “radioscaphoid” and “radiolunate” forces, two forces equal to 100 N were applied: one of them was applied to the ulna side, the other one was applied to the radius side

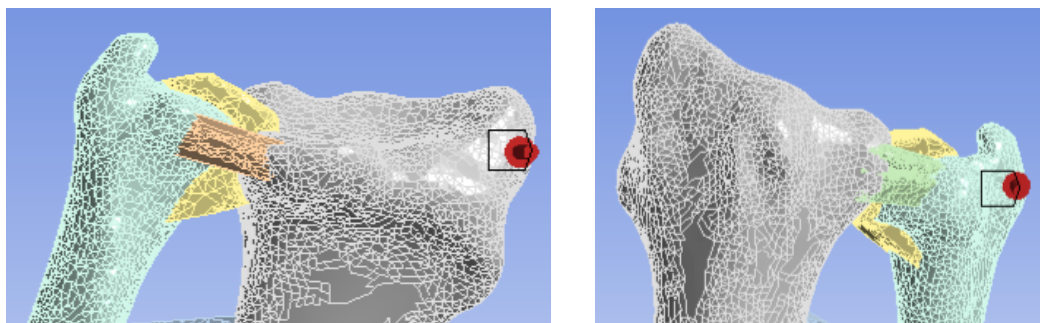


Figure 34. Forces to simulate the twist movement of the joint

## 2.6 Fracture Risk Analysis

To analyze the risk of fracture of bones of two models, a short Matlab program was made to take the young's modulus, previously assigned, and calculated UTS (Ultimate Tensile Strength) of each element of the radius and ulna. In particular, the Ultimate Tensile Strength was the stress at which a material broke.

In steps of creation of bones, two kinds of material were created: cortical and cancellous, so basically there were two values of density and two young's modulus. To apply this program, it was necessary to modify in Mimics the number of materials from 2 to 100. The Matlab code took the density and the young's modulus from the exported Mimics file and calculated the UTS. Then, another short Matlab program was made to take the calculated stress values from models simulated in Ansys, and to compare these stress values to the UTS, calculated previously; if the ratio exceeds 1, then there was a fracture of bones.

## **3. Results**

In this study, two types of analysis were performed with the Finite Element Models:

- Verification of 3D Models, useful to understand if it was correctly realized for subsequently simulations
- Analysis of stress and strain simulations was useful to understand if forces and constrains were applied in a correct way, to re-create the anatomical movements of the DRUJ.

### **3.1 Verification of 3D Models**

A key part of the model to ensure integrity of results was the accurate geometrical model of the articulating surfaces.

After the creation of the radius, ulna and cartilage masks, 3D objects were obtained (see section 2.1); but these objects needed to some improvements in order to obtain geometrical features as much as possible well defined. All this was carried out thanks to the “smooth” and “remesh” tools of the software “3-Matic”

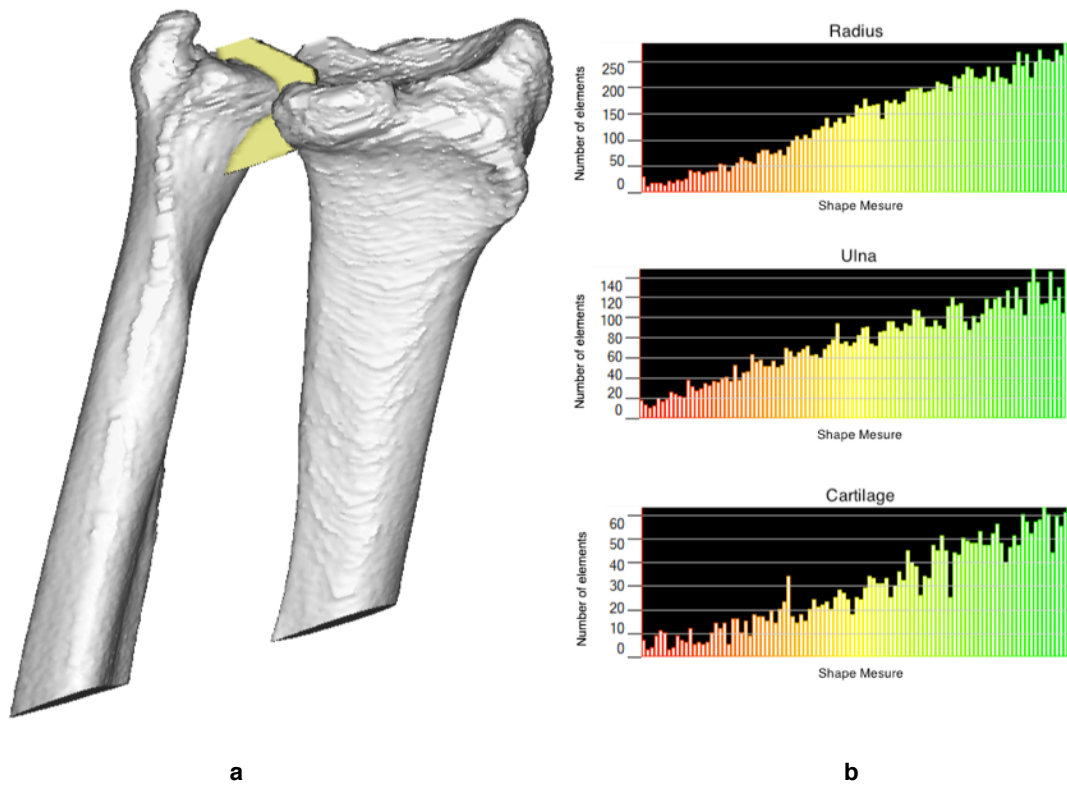


Figure 35. a) Raw Model; b) Histogram of three raw objects of components of the joints

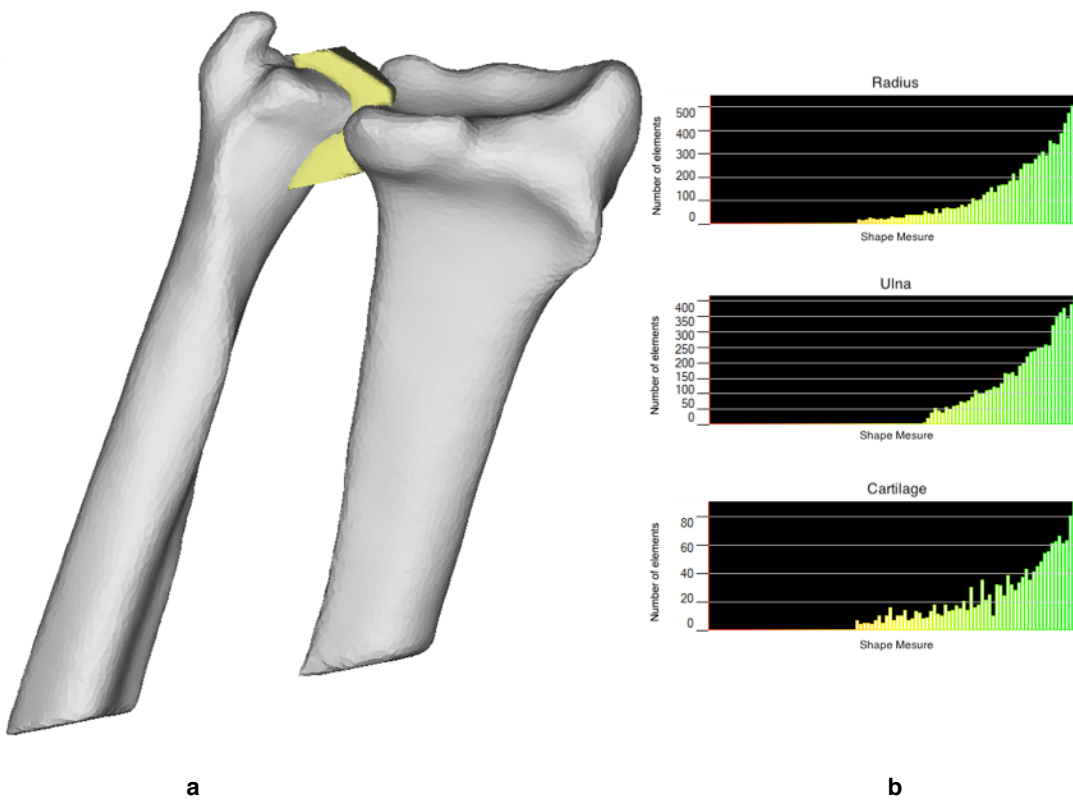


Figure 36. a) Well defined Model; b) Histogram of three well defined objects of components of the joints

In the histograms of each component (Figure 35), it was possible to note the presence of:

- red elements, that represented the not equilateral tetrahedral elements, namely, the most obvious irregularities of components;
- yellow elements, that represented the not perfectly equilateral tetrahedral elements, namely, the less prominent irregularities of components;
- green elements, that represented the equilateral tetrahedral elements, namely, the regular surfaces of components.

In figure 36, further refinement operations, it was possible to observe that the majority of tetrahedral elements taking an equilateral shape because the distribution histogram shifted to the right and only green bars (equilateral tetrahedral elements) were present.

Finally, adding ligaments created by “SolidWorks” (see section 2.3), it was possible to obtain a complete 3D Models of healthy and pathological DRUJ

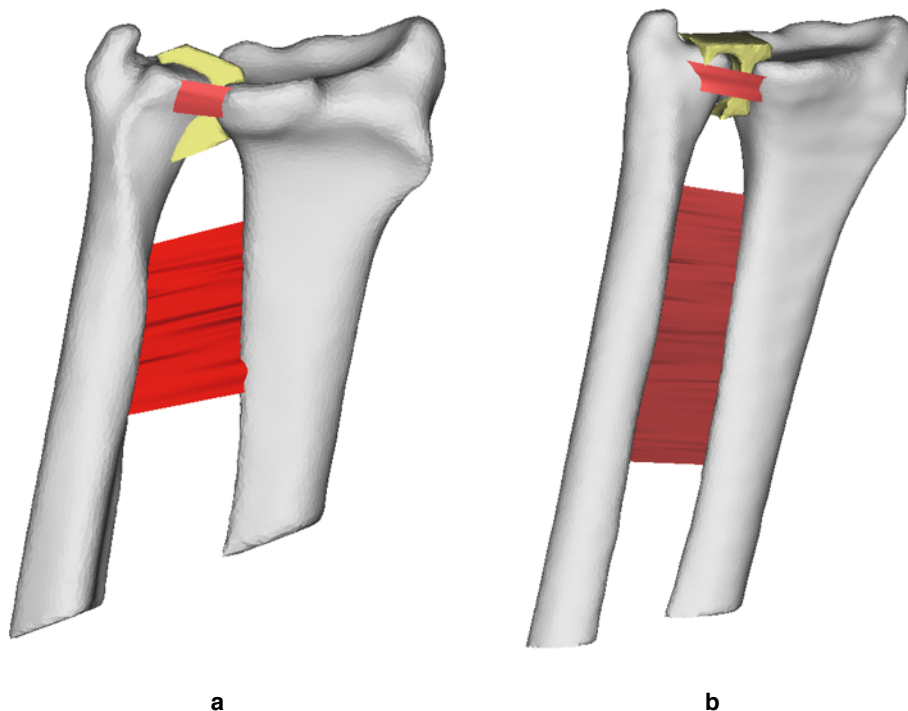


Figure 37. a) Frontside of the complete Healthy Model ; b) Frontside of the complete Pathological



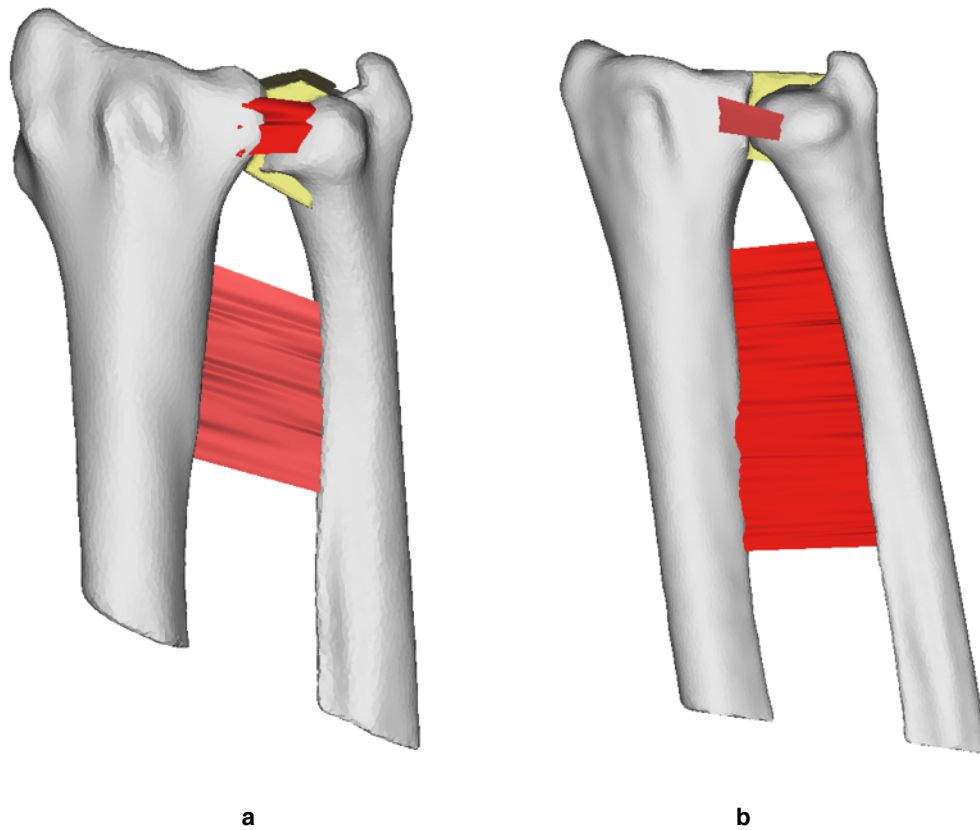


Figure 38. a) Backside of the complete Healthy Model ; b) Backside of the complete Pathological Model

From the figures 37-38, it was possible to observe that imprecisions and irregularities present in the raw models were deleted without being too aggressive and therefore without affecting the geometric features of the components (radius, ulna, and cartilage).

### 3.2 Verification of stress and strain simulations

Stress and strain plots were created of the DRUJ bones and the load transfer characteristics were observed.

In particular, simulations performed for models, were:

- Equivalent (Von-Mises) Stress
- Equivalent (Von-Mises) Strain

The following results were obtained

- Stress

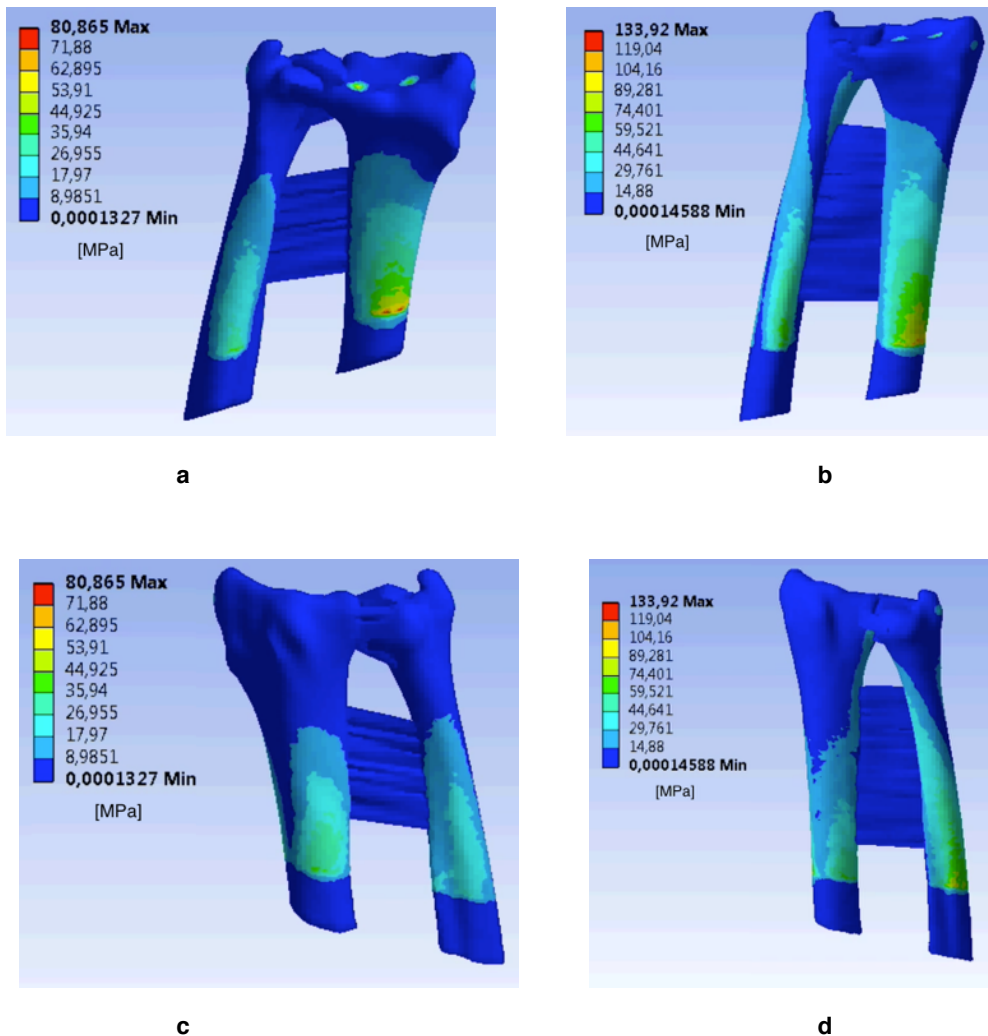


Figure 39. Distribution of the stress: a) Frontside of the Healthy Model; b) Frontside of the Pathological Model; c) Backside of the Healthy Model; d) Backside of the Pathological Model

From the stress plots, it was possible to see that, in the healthy model, maximum tensile stress value of about 80 MPa was achieved, however in the pathological model, maximum stress value of about 130 Mpa was reached. The average values of stress were 40 MPa and 65 Mpa respectively for the model healthy and pathological. In general, in tension, the bone has a modulus of rupture equal to 80-120 MPa.

In this phase of simulation, it was possible to observe that higher values of stress were achieved in the proximal area of the two bones, in

correspondence of the constraints (see section 2.5.1), and in the points in which the forces were applied (see section 2.5.2). The difference between the two models was that the stress, in the pathological model, assumed relevance values also in the area of the distal internal DRUJ.

- Strain

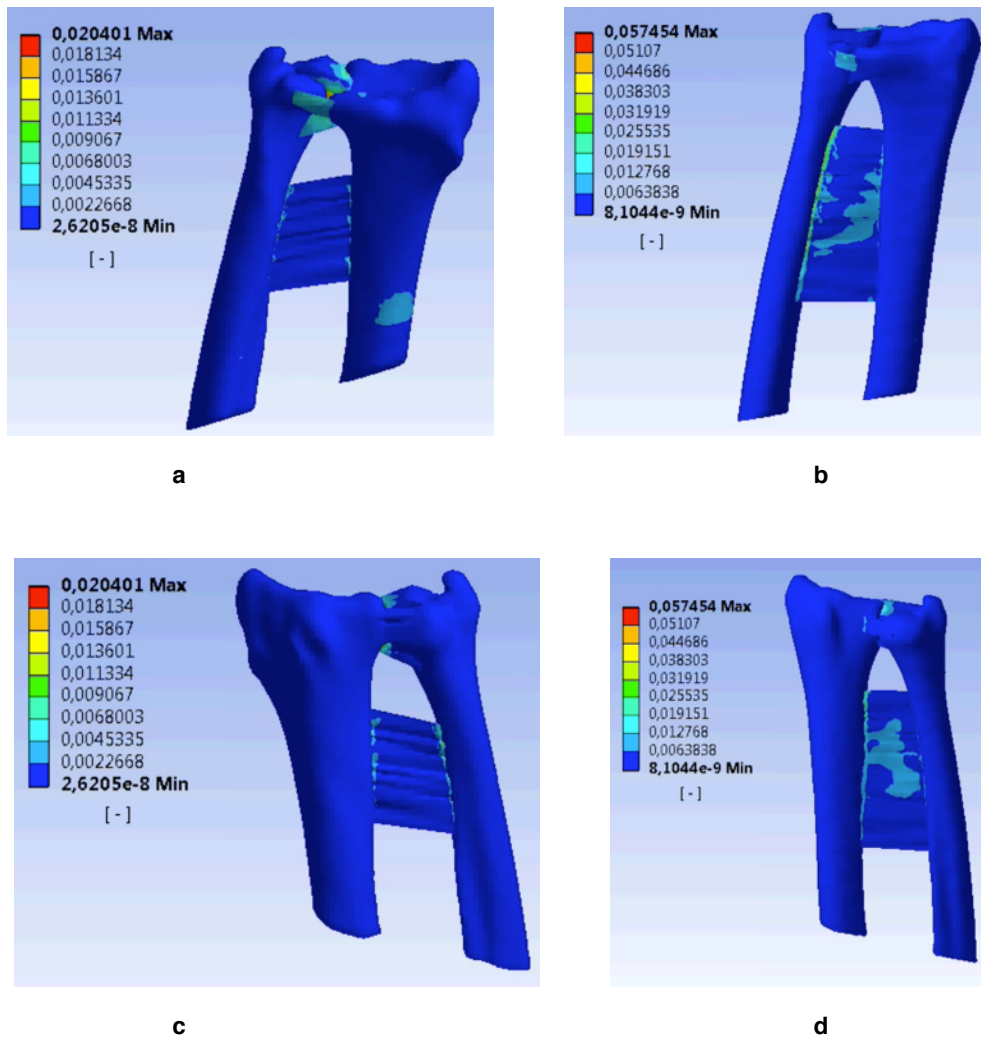


Figure 40. Distribution of the strain: a) Frontside of the Healthy Model; b) Frontside of the Pathological Model; c) Backside of the Healthy Model; d) Backside of the Pathological Model

From the strain plots, it was possible to see that, in the healthy model, maximum tensile strain value of about 0.02 was achieved, however in the pathological model, maximum strain value of about 0.05 was reached. The average values of stress were 0.01 and 0.025 respectively for the model healthy and pathological.

In this phase of simulation, it was possible to observe that in the healthy model, higher values of strain were achieved in the cartilage, palmar ligament and in the areas where the interosseous ligament and two bones were connected; in the pathological model, indeed, higher value of strain were achieved in the cartilage and dorsal ligament (only in the areas close to the radius), in the palmar and interosseous ligament. The main difference between two models was that the strain in the pathological model, assumed relevance values in almost all interosseous ligament.

From both simulations, it was concluded that pathological conditions, in this study the ulnar dislocation, cause different challenging in the Biomechanics of DRUJ.

### 3.3 Clinical Aspects

The study on the biomechanical changes was useful for the clinical aspects. Through an algorithm developed by Matlab (see section 2.6), an analysis of risk fracture was performed.

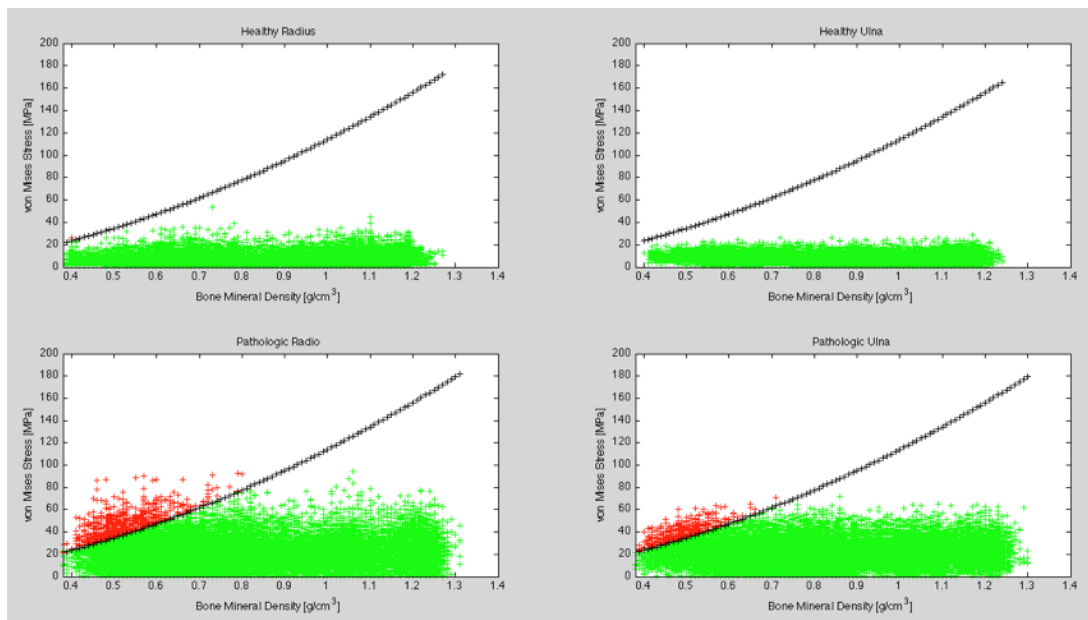


Figure 41. The plots were obtained from the analysis of risk fracture; the green points represented the healthy elements of bones, while the red points represented the pathological elements of bones. In the top, there are two plots that belong to healthy bones, while in the bottom, there are two plots that belong to pathological bones.

From plots above, it was shown that fracture points were occurred only in the pathological model. Plotting the fracture points on the 3D Model, it was possible to observe the distribution of these points

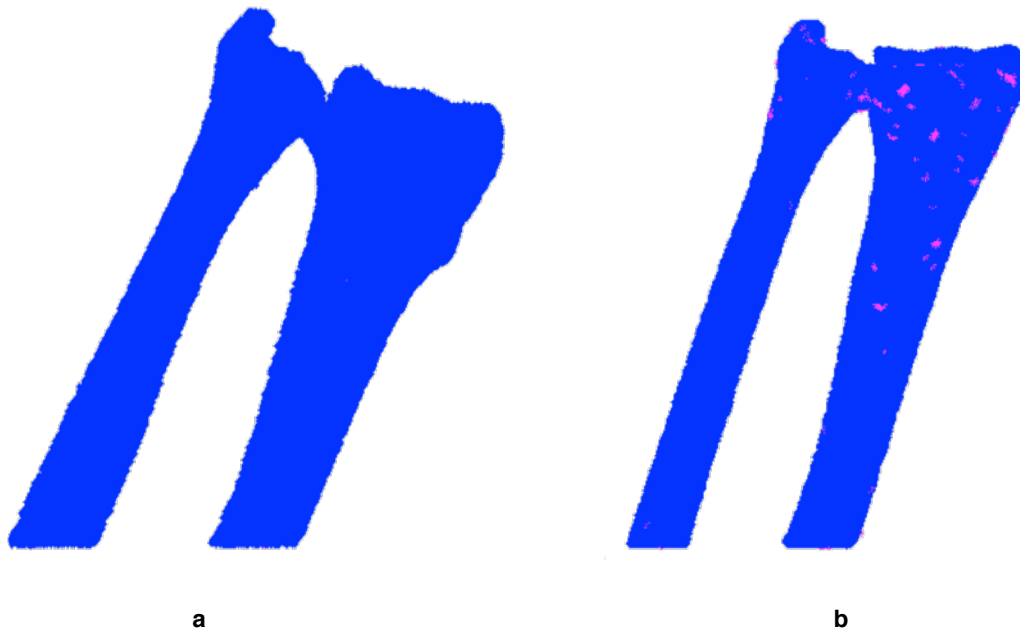


Figure 42. Distribution of fracture points on surfaces of two bones: a) Healthy Model; b) Pathological Model. The fracture points are represented in red colour.

According to the Von-Mises Stress Simulation, the fracture points were mainly distributed in the distal area of DRUJ. In particular, 2% of Radius elements and 1,26% of Ulna elements were classified as fracture risk point. These results demonstrated that applying the same physiological loads in healthy and pathological articulation, in the latter there is an increased risk of bone fracture.

## 4. Discussion

The aim of the project was to evaluate the clinical e biomechanical aspects of the distal radio-ulnar joint, through the use of modeling methods and finite element analysis.

The main steps of this study were:

- Realization of the geometrical models of the joints

A representative and correct geometrical model was useful to design the Finite Element Model. Nowadays, with enhanced scanners and software it is possible to achieve high degree of resolution for a geometrical model. In this study, thanks to “Mimics” software, it was possible to carry out image processing and segmenting in order to create two 3D models.

3D models are designed from DICOM CT-images, that belonged to a patient with healthy joint and a patient with pathologic joint; in particular, the pathology was caused by a traumatic dislocation of the ulna.

The main components of models were: radius, ulna, cartilage, interosseous, palmar and distal ligaments.

Segmentation methods of “Thresholding” and “RegionGrowing” were used to realize the Radius and Ulna bones.

The “Mimics” tools have allowed an automated Segmentation, but it was not enough to capture the full 3D geometry of components of joints, so a manual Segmentation was at times necessary.

In the multi-bone modeling, a high quality of Segmentation could not be underestimated for two reasons:

- The congruence of articulating surfaces is most important in the contact between the components;
- Once the geometry is constructed and meshed, it is very difficult to make any changes to it without starting from the beginning again.

Through the use of masks and morphologic operations, it was possible to create the cartilage and to determinate the distribution between cortical and cancellous bone.

The joints as the wrist, due to the high mobility, needed to be constrained through a set of ligaments to ensure structural integrity of the joint. Without any structural contribution from the ligaments, any finite model of the wrist would diverge.

In this case, ligaments were designed by taking the node-points of the Radius and Ulna, then the area through them is formed.

- Meshing of the models

The quality of the mesh of the Finite Element Model had determined the quality of the solution. The process of meshing was carried out through an automated meshing tool, which had decreased the time and effort to create high quality meshes. In this work, the surfaces were meshed using triangular surface elements.

In general, these elements are capable of capturing a high degree of geometric non-linearity and they are the most popular elements used in biomechanical modeling research today. The problem with the tetrahedral elements is the stiffness of the 4 node tetrahedral element which can give too high stress values compared to the 10 node tetrahedral element. If using a 4 node tetrahedral element, the user must be confident that a sufficient number of elements is being used to capture the nonlinear geometry.

In this study, the elements were 4 node. They have been known to be overly stiff, but since the density of elements was quite high, then it was not occurred.

For each component of two models, the corresponding material properties were assigned. To improve the quality of two models, it was necessary to apply operations of "Smoothing". The "3-Matic" software offered the smoothing tool for 3D objects; it was inevitable to get unsmooth edges, above all where some operation of manual segmentation was required. During the step of smoothing, it was necessary to be aware that this technique could be too aggressive and therefore there could be a loss of volume whilst trying to obtain a good looking picture

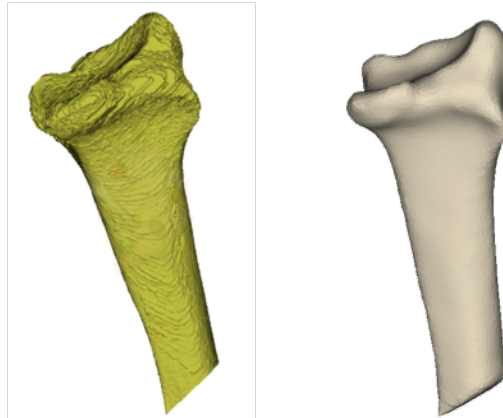


Figure 45. The radius bone before and after three dimensional smoothing

- Finite Element Analysis

A Finite Element Analysis was performed through the use of constraints and forces, which can simulate the behavior of two joints.

Higher values of stress and strain were detected in the pathological joint, consequently, during the stress simulations, radius, ulna and cartilage were most stresses than the healthy joint; during strain simulations, the soft tissues (in particular the interosseous ligament) were more strained. Then, it was possible to deduce that as a result of a traumatic event, the biomechanics of DRUJ is altered.

- Clinical Aspects

The dislocation of the distal radio-ulnar joint is one of the most frequent causes of painful joint limitations. As a result of a fall on the palm of the hand, the twist of forearm creates a disjunction of radio-ulnar joint; subsequently the traumatic impulse could be transmitted to the radius and it fractures. The diagnosis of this injury is often missed, due to unclear clinical signs and occasional difficulties to obtain appropriate images.

In simplest clinical cases, a not cruel reduction maneuver restores the correct location of DRUJ; in more complex cases, a cruel reduction, through surgical intervention, is necessary.



In this thesis, after having reconstructed the DRUJ 3D models and having carried out a Finite Element Analysis, an algorithm was developed in order to know any points at risk of fracture, as a result of the ulnar dislocation.

Indeed, results of this clinical evaluation could be useful to specialists both to detect any fracture points that are not detectable with X-ray or CT-scan, both to facilitate the eventual reduction maneuver.

### *Limitations*

Although good results were obtained, limitations are still present due to the approximation in the construction of the shape of the cartilage and ligaments, not having available MRI images, but only CT, cartilage and ligaments have been created based on the images of the anatomy of the joint.

## 5. Conclusion

Creating a Finite Element Model of the DRUJ and other multibody joints is a complex task where many different aspects of the modeling need to be addressed.

In this study, the most important aspect contributing to a high quality finite element model was the construction of high integrity geometrical model and the soft tissue modeling. High integrity geometrical model of the articulating surfaces aided the contact analysis, while a high degree of incongruence of the articulating surfaces would lead to element distortion. The external soft tissue constraints were important in order to maintain mechanical equilibrium as well as allowing the bones to translate and rotate under loading. These two factors played an integral role in the Finite Element Model.

Using the Finite Element Method predicting the load transfer through the healthy and the pathological joint can give clinicians important information regarding the choice of treatment which can lead to higher procedure success rates and improve the quality of life for many patients.

### *Future work*

Following the already mentioned limitation, in the future it can work to improve the accuracy in the construction of cartilage and ligaments.

Moreover, in this work in a first approximation, the simulations of stress and strain were used , but as already demonstrated (Cristofolini et al. 2010), in the analysis of bone structures, the only simulation of maximum strain should be used because it gives the best information about the break of the bone.

## References

1. Anatomy of Gray vol. 1. Zanichelli, 40<sup>a</sup> edizione,
2. Gupta R1, Allaire RB, Fornalski S, Osterman AL, Lee TQ. Kinematic analysis of the distal radioulnar joint after a simulated progressive ulnar-sided wrist injury.
3. Adams BD. Distal radioulnar joint instability. Instr Course Lect 1998;47:209-213.
4. Linscheid RL. Biomechanics of the distal radioulnar joint. Clin Orthop 1992;17:46-55.
5. Melone CP Jr, Nathan R. Traumatic disruption of the triangular fibrocartilage complex Pathoanatomy. Clin Orthop 1992;10:65-73.
6. Palmer AK, Werner FW. The triangular fibrocartilage complex of the wrist--anatomy and function. J Hand Surg 1981;6:153-162.
7. Tolat AR, Stanley JK, Trail IA. A cadaveric study of the anatomy and stability of the distal radioulnar joint in the coronal and transverse planes. J Hand Surg 1996;21B:587- 594.
8. af Ekenstam F, Hagert CG. Anatomical studies on the geometry and stability of the distal radio ulnar joint. Scand J Plast Reconstr Surg 1985;19:17-25.
9. af Ekenstam F. Osseous anatomy and articular relationships about the distal ulna. Hand Clin 1998;14:161-164.
10. Palmer AK, Werner FW. Biomechanics of the distal radioulnar joint. Clinical Orthopaedics and Related Research 1984.
11. Lees VC, Scheker LR. The radiological demonstration of dynamic ulnar impingement. J Hand Surg 1996;22B:448– 450.
12. Scheker LR, Severo A. Ulnar shortening for the treatment of early post-traumatic osteoarthritis at the distal radioulnar joint. J Hand Surg 2001;26B: 41–44.
13. Pfaeffle HJ1, Fischer KJ, Manson TT, Tomaino MM, Herndon JH, Woo SL. A new methodology to measure load transfer through the forearm using multiple universal force sensors. Journal of Biomechanics 32 (1999).

14. Shaaban H1, Giakas G, Bolton M, Williams R, Scheker LR, Lees VC. The distal radioulnar joint as a load-bearing mechanism--a biomechanical study. *J Hand Surg* 2004.
15. Kihara H, Short WH, Werner FW, Fortino MD, Palmer AK. The stabilizing mechanism of the distal radioulnar joint during pronation and supination. *J Hand Surg* 1995;20A: 930 –936.
16. Shapiro, Linda G. & Stockman, George C. (2002). "Computer Vision". Prentice Hall.
17. *Image Analysis and Mathematical Morphology* by Jean Serra (1982).
18. *Image Analysis and Mathematical Morphology, Volume 2: Theoretical Advances* by Jean Serra (1988).
19. *An Introduction to Morphological Image Processing* by Edward R. Dougherty (1992)
20. *Morphological Image Analysis; Principles and Applications* by Pierre Soille (1999), 2nd edition (2003).
21. *Mathematical Morphology and its Application to Signal Processing*, J. Serra and Ph. Salembier (Eds.), proceedings of the 1st International workshop on mathematical morphology and its applications to signal processing (ISMM'93) (1993).
22. *Mathematical Morphology and Its Applications to Image Processing*, J. Serra and P. Soille (Eds.), proceedings of the 2nd international symposium on mathematical morphology (ISMM'94) (1994).
23. *Mathematical Morphology and its Applications to Image and Signal Processing*, Henk J.A.M. Heijmans and Jos B.T.M. Roerdink (Eds.), proceedings of the 4th international symposium on mathematical morphology (ISMM'98) (1998).
24. *Mathematical Morphology: 40 Years On*, Christian Ronse, Laurent Najman, and Etienne Decencière (Eds.) (2005).
25. *Mathematical Morphology and its Applications to Signal and Image Processing*, Gerald J.F. Banon, Junior Barrera, Ulisses M. Braga-Neto (Eds.), proceedings of the 8th international symposium on mathematical morphology (ISMM'07) (2007).

26. Mathematical morphology: from theory to applications, Laurent Najman and Hugues Talbot (Eds). ISTE-Wiley (520 pp.) June 2010.
27. Zienkiewicz, O.C.; Taylor, R.L.; Zhu, J.Z. (2005). The Finite Element Method: Its Basis and Fundamentals (Sixth ed.). Butterworth-Heinemann.
28. Luca Cristofolini, Enrico Schileo, Mateusz Juszczak, Fulvia Taddei, Saulo Martelli and Marco Viceconti (2010). Mechanical testing of bones: the positive synergy of finite –element models and *in vitro* experiments
29. VicecontiM, DavinelliM, TaddeiF, CappelloA. Automatic generation of accurate subject specific bone finite element models to be used in clinical studies. Journal of Biomechanics 2004;37:1597–605.
30. TaddeiF, PancantiA, VicecontiM. An improved method for the automatic mapping of computed tomography numbers onto finite element models. Medical Engineering and Physics 2004;26:61–9.
31. Finite element model creation and stability considerations of complex biological articulation: The human wrist joint. Gíslason MK1, Stansfield B, Nash DH. Medical Engineering & Physics 32 (2010). pp. 523–531.
32. Garcia-Elias M, Ribe M, Rodriguez J, Cost J, and Casas J: Influence of joint laxity on scaphoid kinematics. Journal of Hand Surgery, 1995, 20B(3): 379–382.
33. Magnús Kjartan Gíslason and David H. Nash. 2012. Finite Element Modelling of a Multi-Bone Joint: The Human Wrist.
34. Nedoma J, Klézl Z, Fousek J, Kestrěánek Z, Stehlík J. Numerical simulation of some biomechanical problems. Mathematics and Computers in Simulation 2003;61:283–95.
35. Schuind F, Cooney WP, Linscheid RL, An KN, Chao EYS. Force and pressure transmission through the normal wrist: a theoretical two-dimensional study in the posteroanterior plane. Journal of Biomechanics 1995;28(5):587–601.
36. AndersonDD, DanielTE. A contact-coupled finite element analysis of the radio- carpal joint. Seminars in Arthroplasty 1995;6(1):30–6.
37. Gíslason M, Nash DH, Nicol A, Kanellopoulos A, Bransby-Zachary M, Hems TEJ, Condon B and Stansfield B.: A Three Dimensional Finite element Model of Maximal Grip Loading in the Human Wrist, Proc. IMechE Part H, Engineering in Medicine, 2009, Vol 223 (H7), 849-862.

38. Guo X, Fan Y and Li ZM: Effects of Dividing the Transverse Carpal Ligament on the Mechanical Behaviour of the Carpal Bones under Axial Compressive Load: A Finite Element Study, *Medical Engineering & Physics*, 2009, 31, 188-194.
39. <http://biomedical.materialise.com/mimics>.
40. <http://biomedical.materialise.com/3-matic>.
41. Tsung-Pao Fang, Les A. Piegl, "Delaunay Triangulation in Three Dimensions", *IEEE Computer Graphics and Applications*, Sept. 1995, vol. 15, no. 5, pp. 62-69.
42. Askeland, Donald R.; Phulé, Pradeep P. (2006). *The science and engineering of materials* (5th ed.). Cengage Learning. p. 198.
41. Beer, Ferdinand P.; Johnston, E. Russell; Dewolf, John; Mazurek, David (2009). *Mechanics of Materials*. McGraw Hill. p. 56.
42. Reddy, J.N. (2005). *An Introduction to the Finite Element Method* (Third ed.). McGraw-Hill.
43. Zienkiewicz, O.C.; Taylor, R.L.; Zhu, J.Z. (2005). *The Finite Element Method: Its Basis and Fundamentals* (Sixth ed.). Butterworth-Heinemann.
44. Felippa, Carlos A. (giugno 2001). A Historical Outline of Matrix Structural Analysis: A Play in Three Acts. *Computers & Structures* (Volume 79, Issue 14, June 2001, Pages 1313-1324).
45. Waterman, Pamela J. (1 agosto 2008). Meshing: the Critical Bridge. *Desktop Engineering Magazine*.
46. Ray W. Clough, Edward L. Wilson, *Early Finite Element Research at Berkeley* (PDF) 2007.
47. Turner, M.J.; R.W. Clough, H.C. Martin, and L.C. Topp (1956). Stiffness and Deflection Analysis of Complex Structures. *Journal of the Aeronautical Sciences* 23: 805–82.
48. Gilbert Strang, George Fix, *An Analysis of the Finite Element Method*, Englewood Cliffs, Prentice-Hall, 1973.
49. Carlos A. Felippa, *Introduction to Finite Element Methods*, Lecture Notes for the course *Introduction to Finite Elements Methods* at the Aerospace Engineering Sciences Department of the University of Colorado at Boulder., from 1976.

50. Carlo Lonati, Gian Carlo Macchi; Dalmazio Raveglia, Crosstalk in a PAM technique telephone switching network due the skin effect. Approach with the Finite Element Method, Conference on the Computation of Magnetic Fields - Proceedings; Laboratoire d'Electrotechnique, Grenoble, 1978.

51. John Leonidas Volakis, Arindam Chatterjee, Leo C. Kempel (1998). Finite element method for electromagnetics: antennas, microwave circuits, and scattering applications. IEEE Wiley Press.

52. Gislason, M.K. , Stansfield, B. , Nash, D.H, Effects of Partial Wrist Arthrodesis on Loading at the Radiocarpal Joints 2009.

## Acknowledgments

I would like to express my gratitude to Prof. Luca Cristofolini, which motivated me to undertake abroad period of study in the faraway and beautiful Iceland. I thank him also for the help and support provided to me during the writing of the thesis work.

I thank Prof. Paolo Gargiulo for having given me the opportunity to realize this thesis and also many other works, which have enriched my professionalism and above all, they gave me the opportunity to becoming aware of my ability. I thank him especially because he allowed me to work in a friendly and informal atmosphere; he has always been available to provide helpful tips and explanations to overcome the problems that I encountered in the development of this work.

I thank Prof. Magnus Kjartan Gislason for availability and courtesy, in particular his indications, that have guided me during the preparation of the thesis, have been precious.

I thank my parents, because they have been my point of reference and with great support, both moral and economic, have allowed me to achieve this important goal.

I heartily thank Joseph Lovecchio which was close to me and has been able to encourage me in difficult times, giving me the right courage and the right moral push.



## Ringraziamenti

Vorrei esprimere la mia gratitudine al Prof. Luca Cristofolini, relatore della mia tesi, per avermi motivata ad intraprendere un periodo di studio all'estero nella lontana e bellissima Islanda; Lo ringrazio, inoltre, per l'aiuto e il sostegno fornitomi durante la stesura del lavoro di tesi.

Ringrazio il Prof. Paolo Gargiulo per avermi dato l'opportunità di realizzare questo lavoro di tesi e anche altri numerosi lavori, che hanno arricchito il mio bagaglio professionale e soprattutto mi hanno dato la possibilità di prendere consapevolezza delle mie capacità. Ciò per cui Lo ringrazio maggiormente, però, è di avermi permesso di lavorare in un clima amichevole ed informale e di essersi sempre dimostrato disponibile a fornirmi utili consigli e spiegazioni per superare i problemi che man mano ho incontrato nello sviluppo del presente lavoro.

Ringrazio il Prof. Magnùs Kjartan Gíslason per la disponibilità e la cortesia avute nei miei confronti, particolarmente preziose sono risultate le sue indicazioni, con le quali sono stata costantemente guidata nell'elaborazione di questa tesi.

Ringrazio i miei genitori, poiché sono stati il mio punto di riferimento e con grande sostegno, sia morale che economico, mi hanno permesso di raggiungere questo importante obiettivo.

Ritengo doveroso rivolgere un grazie di "cuore" a Joseph Lovecchio, che tanto mi è stato vicino e ha saputo incoraggiarmi nei momenti difficili che di volta in volta si presentavano, dandomi il giusto coraggio e la giusta spinta morale.